IEC TR 62396-8

Edition 1.0 2020-04

TECHNICAL REPORT

colour inside

Process management for avionics – Atmospheric radiation effects – Part 8: Proton, electron, pion, muon, alpha-ray fluxes and single event effects in avionics electronic equipment – Awareness guidelines

IEC TR 62396-8:2020-04 (en)

IEC Central Office
3, rue de Varembé
CH-1211 Geneva 20
Switzerland

Tel.: +41 22 919 02 11
info@iec.ch
www.iec.ch

About the IEC
The International Electrotechnical Commission (IEC) is the leading global organization that prepares and publishes International Standards for all electrical, electronic and related technologies.

About IEC publications
The technical content of IEC publications is kept under constant review by the IEC. Please make sure that you have the latest edition, a corrigendum or an amendment might have been published.

IEC publications search - webstore.iec.ch/advsearchform
The advanced search enables to find IEC publications by a variety of criteria (reference number, text, technical committee,…). It also gives information on projects, replaced and withdrawn publications.

IEC Just Published - webstore.iec.ch/justpublished
Stay up to date on all new IEC publications. Just Published details all new publications released. Available online and once a month by email.

IEC Customer Service Centre - webstore.iec.ch/csc
If you wish to give us your feedback on this publication or need further assistance, please contact the Customer Service Centre: sales@iec.ch.

Electropedia - www.electropedia.org
The world's leading online dictionary on electrotechnology, containing more than 22 000 terminological entries in English and French, with equivalent terms in 16 additional languages. Also known as the International Electrotechnical Vocabulary (IEV) online.

IEC Glossary - std.iec.ch/glossary
67 000 electrotechnical terminology entries in English and French extracted from the Terms and Definitions clause of IEC publications issued since 2002. Some entries have been collected from earlier publications of IEC TC 37, 77, 86 and CISPR.

IEC TR 62396-8

Edition 1.0 2020-04

TECHNICAL REPORT

colour inside

Process management for avionics – Atmospheric radiation effects – Part 8: Proton, electron, pion, muon, alpha-ray fluxes and single event effects in avionics electronic equipment – Awareness guidelines

INTERNATIONAL ELECTROTECHNICAL COMMISSION

ICS 03.100.50; 31.020; 49.060

ISBN 978-2-8322-8010-2

Warning! Make sure that you obtained this publication from an authorized distributor.

CONTENTS

INTERNATIONAL ELECTROTECHNICAL COMMISSION

_____

PROCESS MANAGEMENT FOR AVIONICS – ATMOSPHERIC RADIATION EFFECTS –

Part 8: Proton, electron, pion, muon, alpha-ray fluxes and single event effects in avionics electronic equipment – Awareness guidelines

FOREWORD

1) The International Electrotechnical Commission (IEC) is a worldwide organization for standardization comprising all national electrotechnical committees (IEC National Committees). The object of IEC is to promote international co-operation on all questions concerning standardization in the electrical and electronic fields. To this end and in addition to other activities, IEC publishes International Standards, Technical Specifications, Technical Reports, Publicly Available Specifications (PAS) and Guides (hereafter referred to as "IEC Publication(s)"). Their preparation is entrusted to technical committees; any IEC National Committee interested in the subject dealt with may participate in this preparatory work. International, governmental and non-governmental organizations liaising with the IEC also participate in this preparation. IEC collaborates closely with the International Organization for Standardization (ISO) in accordance with conditions determined by agreement between the two organizations.
2) The formal decisions or agreements of IEC on technical matters express, as nearly as possible, an international consensus of opinion on the relevant subjects since each technical committee has representation from all interested IEC National Committees.
3) IEC Publications have the form of recommendations for international use and are accepted by IEC National Committees in that sense. While all reasonable efforts are made to ensure that the technical content of IEC Publications is accurate, IEC cannot be held responsible for the way in which they are used or for any misinterpretation by any end user.
4) In order to promote international uniformity, IEC National Committees undertake to apply IEC Publications transparently to the maximum extent possible in their national and regional publications. Any divergence between any IEC Publication and the corresponding national or regional publication shall be clearly indicated in the latter.
5) IEC itself does not provide any attestation of conformity. Independent certification bodies provide conformity assessment services and, in some areas, access to IEC marks of conformity. IEC is not responsible for any services carried out by independent certification bodies.
6) All users should ensure that they have the latest edition of this publication.
7) No liability shall attach to IEC or its directors, employees, servants or agents including individual experts and members of its technical committees and IEC National Committees for any personal injury, property damage or other damage of any nature whatsoever, whether direct or indirect, or for costs (including legal fees) and expenses arising out of the publication, use of, or reliance upon, this IEC Publication or any other IEC Publications.
8) Attention is drawn to the Normative references cited in this publication. Use of the referenced publications is indispensable for the correct application of this publication.
9) Attention is drawn to the possibility that some of the elements of this IEC Publication may be the subject of patent rights. IEC shall not be held responsible for identifying any or all such patent rights.

The main task of IEC technical committees is to prepare International Standards. However, a technical committee may propose the publication of a Technical Report when it has collected data of a different kind from that which is normally published as an International Standard, for example "state of the art".

IEC TR 62396-8, which is a Technical Report, has been prepared by IEC technical committee 107: Process management for avionics.

The text of this Technical Report is based on the following documents:

Draft TR	Report on voting
107/355/DTR	107/365/RVDTR

Full information on the voting for the approval of this Technical Report can be found in the report on voting indicated in the above table.

This document has been drafted in accordance with the ISO/IEC Directives, Part 2.

A list of all the parts in the IEC 62396 series, published under the general title *Process management for avionics – Atmospheric radiation effects,* can be found on the IEC website.

The committee has decided that the contents of this document will remain unchanged until the stability date indicated on the IEC website under "http://webstore.iec.ch" in the data related to the specific document. At this date, the document will be

- reconfirmed,
- withdrawn,
- replaced by a revised edition, or
- amended.

IMPORTANT – The 'colour inside' logo on the cover page of this publication indicates that it contains colours which are considered to be useful for the correct understanding of its contents. Users should therefore print this document using a colour printer.

INTRODUCTION

Atmospheric radiation can be responsible for causing single event effects (SEEs) in electronic equipment. Beside neutrons and protons, there are other atmospheric radiation sources (for example electrons, pions and muons), which are currently regarded as minor sources, which can also affect electronics in avionics and terrestrial applications. This is currently a new emerging topic with a limited amount of test data and supporting information.

This document, as part of the IEC 62396 series, provides awareness on this new emerging topic in order to inform avionics systems designers, electronic equipment manufacturers and component manufacturers and their customers of the kind of ionising radiation environment that their electronic devices can be subjected to in aircraft and the potential effects this radiation environment can have on those electronic devices.

This awareness is unavoidable due to the aggressive scaling of electronic semiconductor devices to smaller and smaller transistor feature sizes where the impact of these radiation sources can become visible or even significant in the future. For example, some evidence of muon effects has appeared in the literature, in which the impact of muons seems to be negligible at present. This document gives a comprehensive survey on the nature of these particles, atmospheric spectra, induced phenomena and possible testing facilities with their radiation sources; it also provides orientation in order to prepare avionics in the future.

PROCESS MANAGEMENT FOR AVIONICS – ATMOSPHERIC RADIATION EFFECTS –

Part 8: Proton, electron, pion, muon, alpha-ray fluxes and single event effects in avionics electronic equipment – Awareness guidelines

1 Scope

This part of IEC 62396 is intended to provide awareness and guidance with regard to the effects of small particles (that is, protons, electrons, pions and muon fluxes) and single event effects on avionics electronics used in aircraft operating at altitudes up to 60 000 feet (18 300 m). This is an emerging topic and lacks substantive supporting data. This document is intended to help aerospace or ground level electronic equipment manufacturers and designers by providing awareness guidance for this new emerging topic.

Details of the radiation environment are provided together with identification of potential problems caused as a result of the atmospheric radiation received. Appropriate methods are given for quantifying single event effect (SEE) rates in electronic components.

NOTE 1 The overall system safety methodology is usually expanded to accommodate the single event effects rates and to demonstrate the suitability of the electronics for application at the electronic component, electronic equipment and system level.

NOTE 2 For the purposes of this document the terms "electronic device" and "electronic component" are used interchangeably.

Although developed for the avionics industry, this document can be used by other industrial sectors at their discretion.

2 Normative references

The following documents are referred to in the text in such a way that some or all of their content constitutes requirements of this document. For dated references, only the edition cited applies. For undated references, the latest edition of the referenced document (including any amendments) applies.

IEC 62396-1:2016, *Process management for avionics – Atmospheric radiation effects – Part 1: Accommodation of atmospheric radiation effects via single event effects within avionics electronic equipment*

3 Terms, definitions, abbreviated terms and acronyms

For the purposes of this document, the terms, definitions, abbreviated terms and acronyms given in IEC 62396-1 and the following apply.

ISO and IEC maintain terminological databases for use in standardization at the following addresses:

- IEC Electropedia: available at http://www.electropedia.org/
- ISO Online browsing platform: available at http://www.iso.org/obp

3.1 Terms and definitions

3.1.1
AND
logic gate which produces, in digital electronics, an output that is true (1) if both inputs are true (1) and an output false (0) if neither or only one input is true (1)

3.1.2
bipolar action
phenomenon whereby some electrons or holes stay in the bulk of the semiconductor and switch on the parasitic transistor to change the data states in memory elements

3.1.3
charge collection
part of electrons or holes pairs collected into storage nodes

Note 1 to entry: Electrons or holes are generated along with the trajectory of high-energy charged particles. This phenomenon is called charge deposition.

3.1.4
linear energy transfer
LET
rate of decrease with distance of the kinetic energy of an ionizing particle, due to the ionization caused by that particle

Note 1 to entry: LET describes the action of radiation into matter. It is related to stopping power which in nuclear physics is defined as the retarding force acting on charged particles, typically alpha and beta particles, due to interaction with matter, resulting in loss of particle energy.

Note 2 to entry: LET is typically quantified in units of $MeV \cdot cm^2 \cdot mg^{-1}$, to account for the density of the material through which the particle travels.

3.1.5
multi-node transient
MNT
multiple transients (SETs) produced along with a high-energy charged particle or in an area affected by bipolar action

3.1.6
negative-AND
NAND
logic gate which produces, in digital electronics, an output that is false (0) only if all its inputs are true (1) and an output true (1) if one or both inputs are false (0)

[SOURCE: IEC 62239-1:2018, 3.1.22]

3.1.7
negative-OR
NOR
logic gate which produces, in digital electronics, an output that is true (1) if both the inputs are false (0) and an output false (0) if one or both inputs are true (1)

[SOURCE: IEC 62239-1:2018, 3.1.23]

3.1.8
OR
logic gate which produces, in digital electronics, an output that is true (1) if one of both inputs is true (1) and an output false (0) if neither input is true (1)

3.1.9
soft error rate
SER
rate at which a device or system encounters or is predicted to encounter soft errors

Note 1 to entry: Usually, this is expressed as either the number of failures-in-time (FIT) or mean time between failures (MTBF). The unit adopted for quantifying failures in time is called FIT, which is equivalent to one error per billion hours of device operation. MTBF is usually given in years of device operation; to put it into perspective, one FIT equals approximately 1 000 000 000 / (24 × 365,25) = 114 077 times more than one-year MTBF.

3.1.10
radiation induced leakage current
RILC
cumulative effect of ion-induced defects in capacitors with ultra-thin oxides

Note 1 to entry: This phenomenon can be noted in floating gate memory with thin oxide layers; data is stored depending on the number of electrons in the floating gate. When a high-energy charged particle passes through the tunnel oxide between the floating gate and source-drain channel underneath, a conduction path is created along the path and stored electrons flow away, resulting in V_{th} shift or SEU.

3.1.11
(quasi-) monoenergetic neutron
neutron from a well-defined distribution of energies obtained by bombarding high-energy charged particles at a thin metallic target

Note 1 to entry: Monoenergetic neutron beams have a single narrow flux peak at a particular neutron energy. All the neutrons in the beam have energies at or close to the nominal energy.

Note 2 to entry: Quasi-monoenergetic neutron beams have a narrow flux peak at a nominal neutron energy and a tail covering a broad range of energies below the nominal energy. Typically, about half the neutrons have energy close to the nominal energy and about half are in the low-energy tail.

3.2 Abbreviated terms and acronyms

ANITA	Atmospheric-like Neutrons from thick Target
BNCT	boron neutron capture therapy
BNL	Brookhaven National Laboratory (USA)
BOX	buried oxide
BPSG	boron phosphorus silicate glass (also named borophosphosilicate glass)
CAM	content addressable memory
CEA / CVA	Atomic Energy Commission / Centre of Valduc (France)
CEA / DIF	Atomic Energy Commission / “Direction” of military applications Ile de France (France)
CMOS	complementary metal oxide semiconductor
CMOSFET	complementary metal oxide semiconductor field effect transistor
CMP	chemical mechanical polishing
CNL	Crocker Nuclear Laboratory (USA)
CNRF	Cold Neutron Research Facility
CPU	central processing unit
CYRIC	CYclotron and RadioIsotope Center (Tohoku University, Japan)
DD	displacement damage
DICE	dual interlocked storage cell
DMR	double modular redundancy
DRAM	dynamic random access memory
DUT	device under test

ECC	error correction code / error checking and correction
ECU	electronic control unit
EEPROM	electrically erasable programmable read-only memory
EMI	electro-magnetic interference
FD	fully depleted
FET	field effect transistor
FF	flip-flop
FIT	failure in time
FNL	Fast Neutron Laboratory (Tohoku University, Japan)
FPGA	field-programmable gate array
GPU	graphic processing unit
HKMG	high-k metal gate
HLA	hyper low alpha
IGBT	insulated gate bipolar transistor
INC	intra nuclear cascade
IUCF	Indiana University Cyclotron Facility (USA)
J-PARC	Japan Proton Accelerator Research Complex (Japan)
L1 / L2	level 1 / level 2 (related to microprocessor cache memories, "level 1" cache memory being usually built onto the microprocessor device itself, “level 2” cache memory being usually on a separate device or expansion card) [SOURCE: IEC TR 62396-7:2017, 3.2]
L3	level 3 (related to, “level 3” cache memory being usually built onto the CPU module or motherboard and working together with L1 and L2 cache memories for improving processing performance
LANSCE	Los Alamos National Science Center (USA)
LAMPF	Los Alamos Meson Physics Facility (USA)
LBNL	Lawrence Berkeley National Laboratory (USA)
LENS	low-energy neutron source (university-based pulsed neutron source at IUCF)
LET	linear energy transfer
MBU	multiple bit upset
MCU	multiple cell upset
MCBI	multi-coupled bipolar interaction
MF	masking factor
MNT	multi-node transient
MOSFET	metal oxide semiconductor field effect transistor
MTBF	mean time between failures
NAND	negative-AND
NIST	National Institute of Standards and Technology (USA)
NMIJ	National Metrology Institute (Japan)
NOR	negative-OR
NPL	National Physical Laboratory (UK)
NYC	New York City
PCB	printed circuit board
PD	partially depleted
PDSOI	partially depleted SOI

PLL	phase locked loop
QMN	quasi-monoenergetic
RAM	random access memory
RCNP	Research Center for Nuclear Physics (Japan)
RILC	radiation induced leakage current
ROM	read only memory
SBU	single bit upset
SEB	single event burnout
SEE	single-event effect
SEFI	single event functional interrupts
SEGR	single event gate rupture
SEL	single event latch-up
SER	soft error rate
SET	single event transient
SEU	single event upset
SIMS	secondary ion mass spectrometry
SOI	silicon on insulator
SRAM	static random access memory
SRIM	stopping and range of ions in matter (related to a collection of softwarepackages
STI	shallow trench insulator
TAMU	Texas A&M University (USA)
TID	total ionization dose
TMR	triple modular redundancy
TSL	The Svedberg Laboratory (Uppsala university, Sweden)
ULSI	ultra large scale integration

4 Technical awareness

4.1 Basic knowledge of atmospheric secondary particles

Primary cosmic rays, which are ionizing particles with extremely high energies, come from the galactic core and the sun to the atmosphere of Earth, where they generate secondary cosmic radiation. The atmospheric radiation environment under normal conditions is described in IEC 62396-1, extreme space weather conditions, which can occur at times of high solar activity, are described in IEC TR 62396-6. Here, an abbreviated description is given, based on terrestrial radiation effects in ULSI electronic components and electronic systems, see [1][1].

Primary cosmic rays in outer space consist mainly of protons. Cosmic rays are charged particles so that they twine around lines of geomagnetic or heliomagnetic forces as illustrated by Figure 1. Some are trapped by geomagnetic force to form the Van Allen radiation belt. Cosmic rays with energies less than a geomagnetic rigidity cut-off tend to be deflected before entering the atmosphere. Some are, on the other hand, attracted into geomagnetic poles along with lines of geomagnetic force sometimes accompanied by aurorae. Cosmic rays are deflected rather strongly near the equator since the lines of geomagnetic force are roughly parallel to the surface of Earth. Therefore, the strength of cosmic rays that reach the atmosphere differs depending on geomagnetic latitude.

[1] Numbers in square brackets refer to the Bibliography.

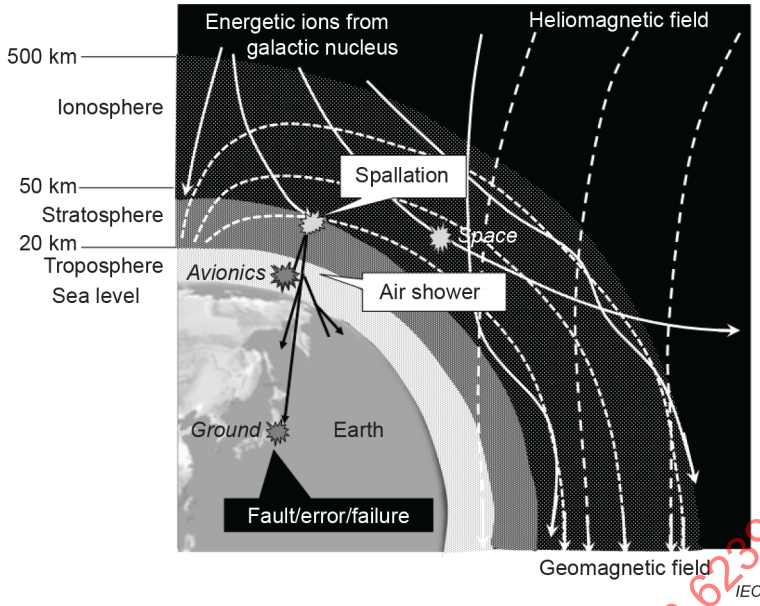

Figure 1 – Cosmic rays as origin of single event effects

When primary cosmic rays enter the atmosphere (troposphere and stratosphere) of Earth, some particles induce spallation reaction in nuclei in the atmosphere (mainly nitrogen and oxygen nuclei) to produce a number of secondary particles including electrons, muons, pions, protons and neutrons as illustrated by Figure 2. Since secondary neutrons in the atmosphere have a longer range than protons, they can cause cascades of spallation reactions in the atmosphere to make air showers that can reach the surface of Earth. Figure 3 shows an estimated differential neutron spectrum at the NYC sea level based on the measured data in JEDEC JESD89 [2]. As the air can shield neutrons, the strength (flux and energy) of neutrons depends upon altitude with a slight dependency on atmospheric pressure [3].

As cosmic rays are also deflected by the heliomagnetic field, which is affected by cyclic solar activity for a period of around eleven years, the strength of neutrons on the ground also has an eleven-year cycle as illustrated by Figure 4. At solar maximum, neutron intensity on the ground is weakest, while it is the strongest at the solar minimum. Under normal activity, the sun emits a large quantity of protons but their energies are relatively low, as shown in Figure 5 for solar maximum conditions, as protons from the sun do not cause air showers on the ground. However, when big flares take place on the sun's surface, a much larger quantity of protons is emitted with comparable energies to galactic protons and can cause air showers.

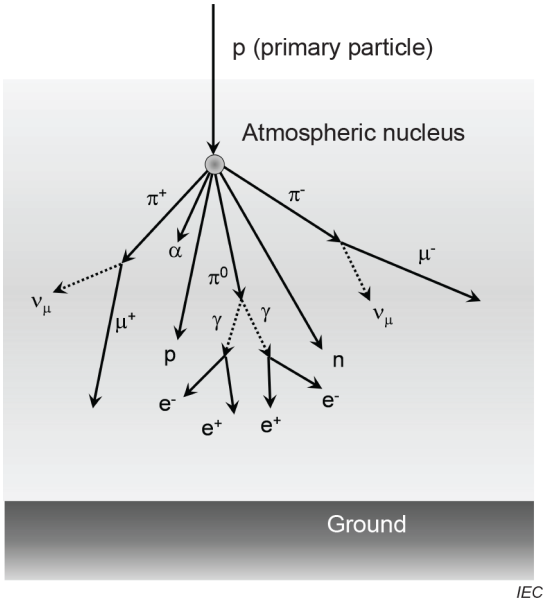

Figure 2 – Initial stage of secondary particle production

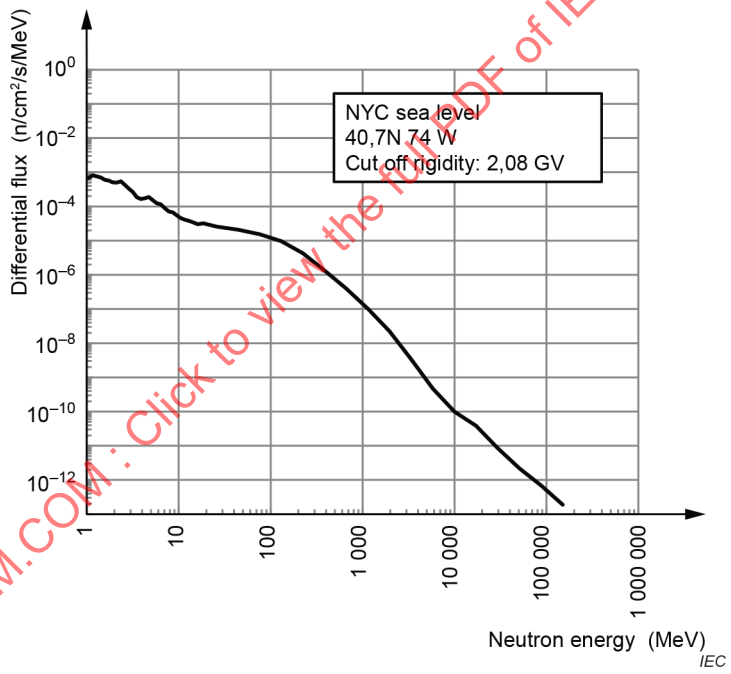

Figure 3 – Differential high-energy neutron spectrum at sea level in NYC

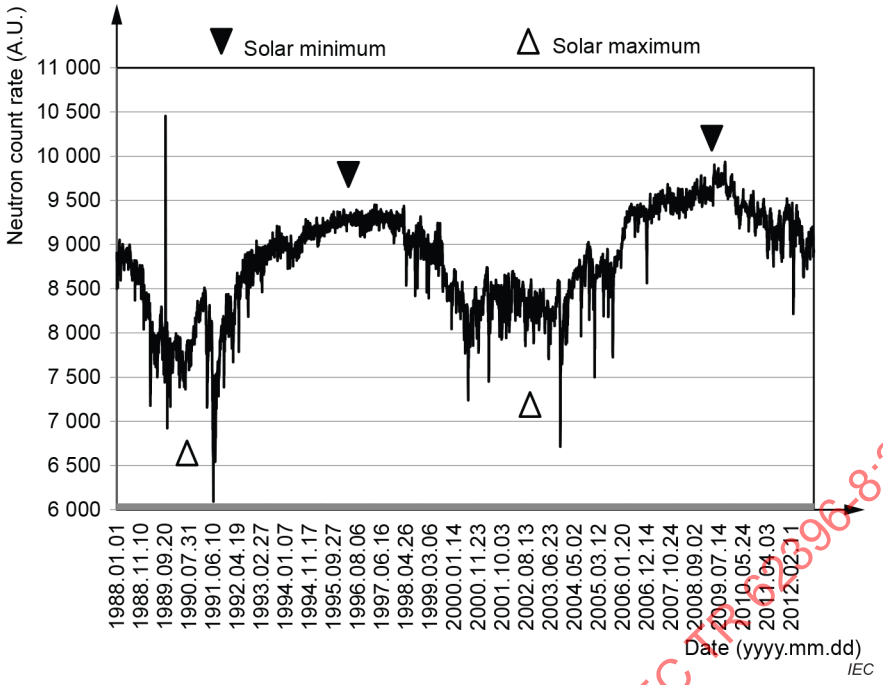

Figure 4 – Long-term cyclic variation in neutron flux measured at Moscow Neutron Monitor Center

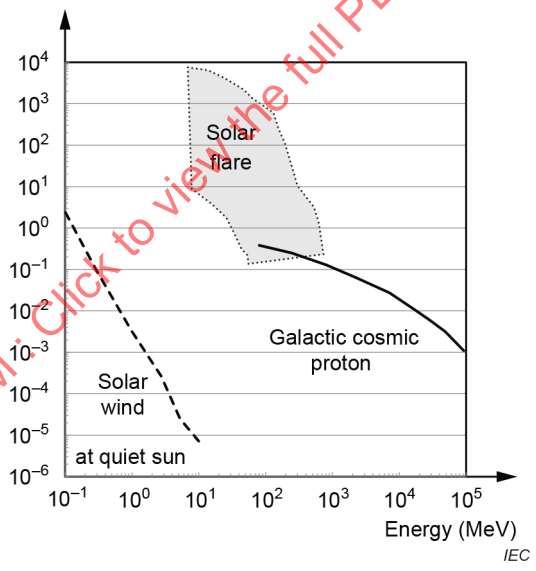

Figure 5 – Differential proton spectra originating from solar-minimum sun, from big flares on the sun, and from the galactic core

4.2 Four typical hierarchies of faulty conditions in electronic equipment: Fault – error – hazard – failure

Electronic equipment can be disrupted by a range of radiation effects [4, 5, 6, 7, 8]. The types of faults caused by atmospheric radiation are summarized in Table 1. Other types of faults are not considered here. Radiation effects can be categorized as cumulative or random, the former comprising effects due to total ionizing dose (TID) and displacement damage (DD); the latter comprising single-event effects (SEEs), of which there are many types. Unlike in space, where electronic equipment encounters high radiation doses from primary cosmic rays and trapped radiation belts, avionics electronic equipment is normally only affected by SEEs, which are equally likely at any time during the operational lifetime of a product, largely irrespective of the accumulated dose.

SEEs originate from spurious transient charge generation in an electronic device well or substrate, caused by the passage of an energetic ionizing particle. Starting from such transients, a kind of hierarchy of fault conditions can be considered as illustrated by Figure 6. When a fault is captured and causes data flips in memory devices such as SRAMs, DRAMs, flash memories and FFs, it is regarded as an error at the electronic device or circuit level. A fault does not always cause an error, depending mainly on the location and the amount of charge collected by an active node. When an error propagates to the final output of an electronic equipment and causes malfunction of the electronic equipment, this consequence is called a failure. An incorrect output of the electronic equipment is called a hazard, especially where it has potential to cause damage. Usually a failure is not recovered by the electronic equipment without physical or economic damage. Failures include shut-down and abnormal operation of the electronic equipment. Incorrect calculations can also be categorized as failures. An error does not always cause an electronic equipment hazard or failure, because it can disappear or be masked during propagation in the device or board by some masking effects. Some mitigation techniques like parity, ECC, and memory interleaving can be applied to reduce the likelihood of error propagation.

Single-event effects occur as a result of a single particle penetrating a device; such a single particle can nonetheless cause more than one error. For example, a single bit-flip is known as a single-event upset (SEU); when a single particle causes multiple bit-flips, this is known as a multiple-cell upset (MCU). Nonetheless, an MCU is still defined as an SEE, because it was caused by a single particle. The fact that single particles cause the effects under consideration is central to the statistical analysis of SEEs. An important aspect to note is that the soft error rate (SER) in this case is defined by the number of SEUs, not by the number of errors. See IEC 62396-1 for more details.

NOTE 1 Informative Annex A describes the structure of CMOS semiconductor devices

NOTE 2 Informative Annex B describes the interaction of particles with CMOS semiconductor devices.

Table 1 – General modes of faults

Type	Definition	Phenomenon	Name	Characteristics	Source	Affected area	In-situ detection method	In-situ recovery/ mitigation method
Transient/ noise	Transient in electric potential and/or current in a chip	Single-event effects (SEEs)	Single event transient (SET)	Single transient due to charge collected by the diffusion layer in the chip. Pulse width is below a few nanoseconds, and can last more than two clock pulses. It can result in different effects (SEU, SET, SEFI, SEB…) depending on the electronic device and the usage conditions.	Well/ substrate	Random but limited to a single well	Time and/or space redundancy such as double/triple modular redundancy (DMR/TMR)	Time and/or space redundancy
			Single event upset (SEU)	Data flip in memory elements (SRAM DRAM, flip-flop, flash memory etc.) by a single particle hit.			Error correction code (ECC)/parity	
			Multi-node transient (MNT)	Simultaneous SETs in more than two diffusion layers. Mainly, MNTs take place in a single well due to charge sharing or bipolar action. Space redundancy techniques such as dual interlocked storage cell (DICE) or TMR might not work against MNTs.			Monitoring the well potential and/or current	Reboot
			Multiple cell upset (MCU)	Data flips in multiple memory elements by a single particle hit.			ECC/parity	Rewrite/ reboot
			Radiation induced leakage current (RILC)	When a charged particle passes through a thin tunnel oxide, a leakage path is formed in the tunnel oxide and the potential in the oxide can rise, resulting in a change in the effective V_{th} and causing a soft error.	Very thin oxide under high electrical stress	Random but limited to tunnel oxide	ECC/parity	ECC
- (Not deterministic)			Single event functional interrupt (SEFI)	Loss of functionality in an electronic circuit. It can be recovered by restoring flip-flop (FF) data to default values.	Well/substrate	Random in a small area	Instruction exception at CPU level	Restoring FF data
	Large destructive current in a channel or through oxide film		Single event latchup (SEL)	Current continues to flow flipping multiple cell data. It can be recovered by power cycling (power off and on).	(Parasitic) PNP junctions	Two-dimensional multiple cells	Monitoring the well potential and/or current	Power cycling
Permanent effects			Single event burnout (SEB)	Destructive bipolar effect in a semiconductor channel particularly in a power device.	PNP junctions	Random in a small area	Monitoring the well potential and/or current	Derating operating voltage
			Single event aate rupture (SEGR)	Destructive effect on oxide films particularly in a power device.	Oxide films under high electrical stress	Random in a small area	-	Derating operating voltage
Cumulative effects	Lattice defects	Displacement damage (DD)		Damage or interstitials in a crystal, which can deteriorate device functionality. Can cause bits to stick at “0/1”and can be permanent.	Anywhere/ tunnel oxide	Random in a small area	-	Annealing can work
	Hole trap/impurity migration	Total ionizing dose (TID) effects		Parasitic levels due to traps/impurities can cause functional deterioration or potential shift.	Oxide	Random in a small area	V_{th} measurement	Annealing can work

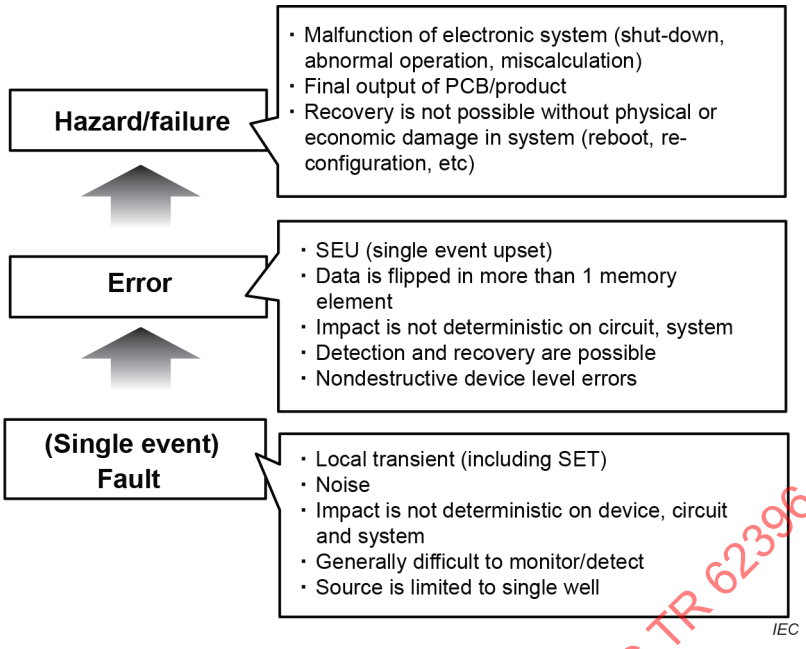

Figure 6 – Typical hierarchy of fault conditions: Fault-error-failure

SEE rates can be quantified by means of a cross section, σ_{SEE}, defined by:

$$\sigma_{SEE} = \frac{N_{SEE}}{\Phi_p} \quad (1)$$

where:

N_{SEE} is the number of SEU events;

Φ_p is the fluence of particles (cm^{-2}).

NOTE 1 Fluence means the total number of particles passing through a unit area.

NOTE 2 σ_{SEE} is expressed in cm^2, which can be per device or, for memory devices, per bit ($cm^2 \cdot b^{-1}$).

The cross section can be measured thanks to accelerator experiments and one can calculate a corresponding failure in time (FIT) rate as follows:

$$FIT = \sigma_{SEE} \times \phi_p \times 1 \times 10^9 \quad (2)$$

where:

ϕ_p is the flux of particles (particles h^{-1} cm^{-2}).

NOTE 3 Flux means the number of particles passing through a unit area per unit time.

NOTE 4 FIT (failure in time) means the number of failures that can be expected in 10^9 h of operation.

4.3 General sources of radiation

4.3.1 General sources of terrestrial radiation

Figure 7 depicts two simplified mechanisms by which ionizing radiation can be produced.

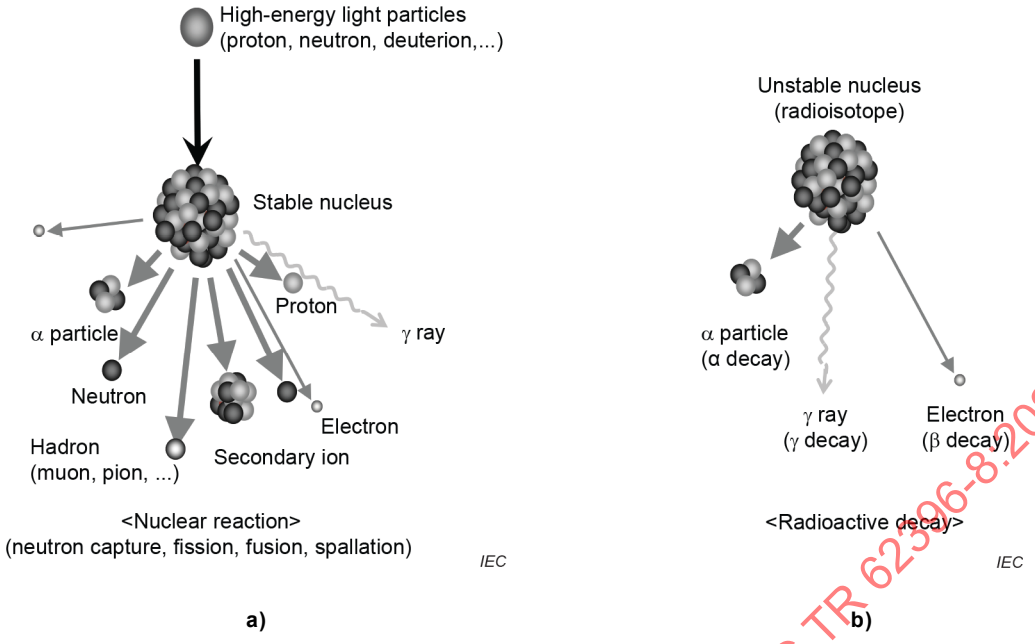

Figure 7 – Sources of atmospheric ionizing radiation: Nuclear reactions and radioactive decay

4.3.2 Atmospheric radiation particles

The particles listed in Table 2 participate in cosmic radiation showers and can cause interactions with electronic components.

Table 2 – Properties of atmospheric radiation particles

article	Symbol	Mass /MeV	Charge	Spin	Mean lifetime /s	Main decay mode[a]
Photon	γ	0	0	1	stable	not applicable
Electron	e^- (β^-)	0,511	−1	½	stable	not applicable
Positron (anti-electron)	e^+	0,511	1	½	stable	not applicable
Muon	μ^-	105,66	−1	½	$2{,}2 \times 10^{-6}$	$\mu^- \rightarrow e^- + \nu_\mu + \bar{\nu}_e$
	μ^+	105,66	1	½	$2{,}2 \times 10^{-6}$	$\mu^+ \rightarrow e^+ + \bar{\nu}_\mu + \nu_e$
Pion	π^+	139,57	1	0	$2{,}6 \times 10^{-8}$	$\pi^+ \rightarrow \mu^+ + \nu_\mu$
	π^-	139,57	−1	0	$2{,}6 \times 10^{-8}$	$\pi^- \rightarrow \mu^- + \nu_\mu$
	π^0	139,57	0	0	$8{,}4 \times 10^{-17}$	$\pi^0 \rightarrow 2\gamma$
Proton	p^+	938,27	1	½	stable	not applicable
Neutron	n^0	939,57	0	½	$8{,}8 \times 10^{2}$	$n^0 \rightarrow p^+ + e^- + \bar{\nu}_e$
Alpha	α	3 733	2	0	stable	not applicable

[a] ν: neutrino, $\bar{\nu}$ anti-neutrino.

Charged particles, such as alpha particles, cause ionization directly and can cause SEE as they do so. In general, for a given particle energy, particles are more highly ionizing if they carry more charge, and the heavier they are. Ionizing particles are most highly ionizing at low energies, close to their Bragg peaks. A high-energy particle is relatively low ionizing, because its high velocity leads to a minor influence on the atoms it passes, and it slows down only gradually as it passes through material, for example aircraft components or the semiconductor material of an electronic device. As it slows, however, its ionizing power increases such that, eventually, it reaches a point where it stops and delivers its remaining kinetic energy over a very short distance. This is the Bragg peak, the ionizing power of which is dependent on the charge state of the particle, the energy at which it occurs depending on the particle mass.

Avionics electronic equipment, therefore, can be affected by that portion of the ionizing particles in the external atmospheric radiation field that has sufficient energy to penetrate a structure and reach an electronic component, but not so much energy that it passes through a structure without stopping.

The energy used in ionization by an ionizing particle can be described by its linear energy transfer (LET), normally expressed in units of $MeV \cdot cm^2 \cdot mg^{-1}$. LET depends on particle energy, mass, and charge state and is greatest at the particles' Bragg peak, close to the point at which it stops. In silicon, the peak LET is approximately 1,4 $MeV \cdot cm^2 \cdot mg^{-1}$ for an alpha particle and 0,5 $MeV \cdot cm^2 \cdot mg^{-1}$ for protons, pions, and muons [9]. Since an average energy of 3,6 eV is required to produce a single electron-hole pair in silicon, which has a density of 2,33 $g \cdot cm^{-3}$, for a LET of value $"X"$ (in units of $MeV \cdot cm^2 \cdot mg^{-1}$) the charge deposition per unit length is ten times $"X"$ (in units of $fC \cdot m^{-1}$). For alpha particles, the maximum charge deposition is 14 $fC \cdot m^{-1}$, for protons, pions and muons it is 5 $fC \cdot m^{-1}$. The energy at which this maximum peak occurs in silicon is approximately 0,5 MeV for alpha articles, 50 keV for protons, and 8 keV for pions and muons. This means than an alpha particle can deposit about 30 fC in silicon at its Bragg peak, a proton about 3 fC, and a pion or muon about 0,5 fC. Electrons and positrons are less ionizing than pions and muons.

Alpha particles are well known to cause SEE when emitted by radioactive decay of contaminants in electronic device packages and solder balls, as illustrated by Figure 7b). Alpha particles are not very penetrating, however, and only the most energetic particles in the atmospheric radiation field surrounding an aircraft are likely to reach the electronic components of avionics electronic equipment. Alpha particles are considered in 4.4.2.

Protons are much more penetrating than alpha particles. Recent evidence shows that electronic devices with silicon feature sizes below 90 nm (called deep-submicron) can be upset by ionization caused by low-energy protons. Protons are considered in 4.4.3.

Low-energy muons and charged pions are similarly penetrating and have similar ionizing power, although less so than protons for a given energy. Tests in muon and pion beams have shown that these particles are capable of causing SEE in some circumstances, especially for electronic devices with very small silicon feature sizes below 20 nm, and that this might be a concern for some future technologies. Muons and pions are considered in 4.4.4.

Electrons and positrons have still less ionizing power than muons and pions, and are not expected to be significant for SEE, even for very small silicon feature sizes below 20 nm [10].

Of the uncharged particles, neutrons are well known to cause SEE. The mechanism for this is indirect: neutrons can cause nuclear interactions to occur inside a semiconductor device (Figure 7a)), causing heavily ionizing particles to be released at energies close to their Bragg peaks. This makes neutrons the principal SEE threat to avionics electronic equipment because they are simultaneously highly penetrating, being uncharged, and potentially highly ionizing, albeit indirectly. High-energy neutrons, with energies conveniently measured in megaelectronvolts, can interact in this way with any kind of material, releasing much of their kinetic energy as ionizing energy. Low-energy neutrons, generally those which have reached thermal equilibrium with their surroundings ("thermal" neutrons) with energies conveniently measured in millielectronvolts, can interact exothermically with boron-10, which is present in

some electronic devices, releasing up to 2,8 MeV of ionizing energy in doing so and generating up to 124 fC charge in silicon. Neutrons are considered in 4.4.5 and 4.4.6.

Other particles, too, can cause nuclear interactions. The first of these are protons, which therefore also form a two-pronged threat to avionics electronic equipment: low-energy protons can cause SEE by direct ionization and high-energy protons can cause SEE indirectly. In addition, negative pions and muons can be captured by an atomic nucleus, leading to an atomic disintegration which can liberate highly ionizing particles, leading to SEE.

Of the other particles listed in Table 2, photons (gamma rays), which are highly penetrating, can release individual electrons through the photoelectric effect at relatively low energies, energize electronics through Compton scattering, or generate electron-position pairs through pair production at high energies. If the gamma flux is sufficiently high, cumulative effects can be significant, but this is not the case in the atmospheric radiation environment. Gamma rays have no direct effect on SEE; whatever small effect there might be can only be mediated through electrons.

Neutrinos arising from muon or pion decay have very weak or no interactions with matter and so do not cause fault conditions in electronics.

Pions, muons, and free neutrons are unstable. Neutron lifetimes are so long, however, that this effect can be neglected in SEE analyses: even thermal neutrons can travel several kilometres in a mean neutron lifetime. At the other extreme, neutral pions only travel a few nanometres on average before decaying and enhancing the gamma flux. Neutral pions, therefore, are not directly relevant for SEE. Charged pions, with typical lifetimes in the order of 10 ns, typically travel a few metres before decaying to enhance the muon flux. Muons, with typical lifetimes in the order of 1 µs, are likely to travel a few hundred metres before decaying to enhance the electron flux. In some cases, muons can be a significant proportion of the atmospheric radiation field, as discussed in 4.3.3.

Spallation interactions between protons and neutrons and the host material of an electronic device, which can lead to SEE, are the same kind of reactions as those between cosmic ray particles (mostly protons) and atmospheric molecules that are the cause of atmospheric radiation.

To analyze radiation effects due to atmospheric radiation particles, knowledge of the flux and energy spectrum of each particle type is important. Table 3 presents selected sources of data or evaluation methods for the spectra of each particle. Data are available from several sources. For neutrons, IEC 62396-1 and JEDEC JESD89 [2] define standard spectra for avionics and ground-level applications, respectively. More generally, environmental data are available from the freely available tools EXPACS [11], derived from PHITS [12], and MAIRE [13]. Thermal and epi-thermal neutron spectra are very strongly dependent on surroundings, and are significantly affected by the presence of aircraft materials and even weather conditions. More information can be obtained from IEC 62396-5, Nakamura et al. [3] and Ziegler and Puchner [14].

Table 3 – Selected data sources for spectra of atmospheric radiation particles

Particle	Source	Note
High-energy neutron	IEC 62396-1, [2] [11] [13]	Indirectly ionizing. Neutrons with energies above a few MeV energy range and above deposit ionizing energy through nuclear interactions with device materials.
Thermal/epi-thermal neutron	IEC 62396-5, [3] [13] [14]	Indirectly ionizing. Low-energy neutrons can release energy through nuclear reactions with boron-10 only. Thermal and epi-thermal neutron spectra are strongly dependent on weather conditions and surrounding materials.
Proton	[11] [13]	Directly ionizing. Protons with energies above a few MeV can also cause indirect ionization through nuclear interactions with device materials
Muon	[11] [13]	Directly ionizing. Negative muons can also release ionization energy through muon capture by device materials.
Helium ion	[11] [13]	
Electron	[11] [13]	
Pion	[13]	
Photon	[13]	

4.3.3 Spectra at the avionics altitude

Figure 8 shows energy-differential flux at 10 000 m altitude above NYC sea level for neutrons, protons, muons, and electrons, calculated using EXPACS. In this energy range (1 MeV to 10 GeV), neutrons have the highest flux. In general, electrons have about one order of magnitude less flux than neutrons. Muon flux is much less than neutron flux below 100 MeV but approaches or slightly exceeds neutron flux above 2 GeV.

NOTE The altitude of 10 000 m is used here for convenience. It differs slightly from that used in IEC 62396-1 (12 160 m, 40 000 ft).

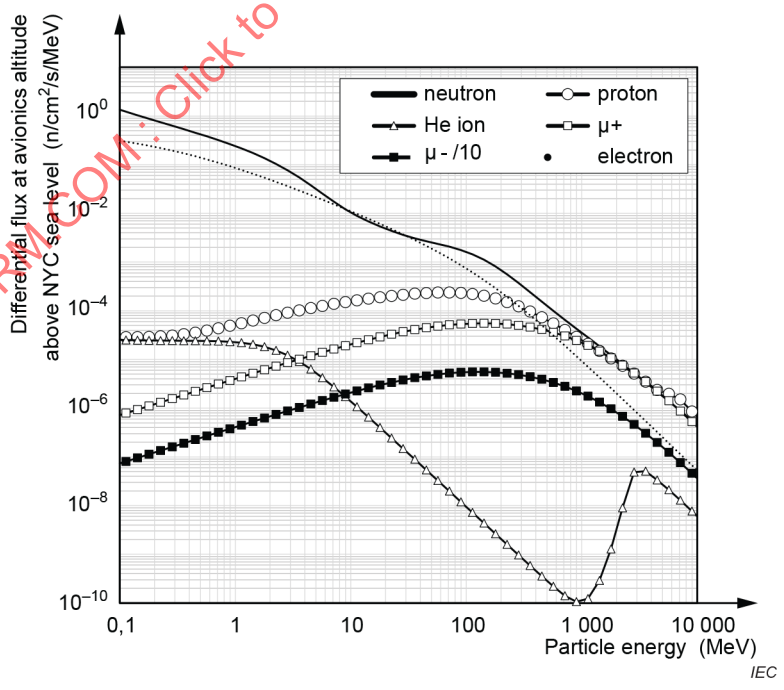

Figure 8 – Differential flux of secondary cosmic rays at avionics altitude (10 000 m) above NYC sea level

Figure 9 shows differential flux at NYC sea level calculated using EXPACS along with some data for pions [14]. It is clearly seen by comparison with Figure 8 that the flux levels are much lower than those at avionics altitude by a factor of 100 to 300. Differential fluxes for neutrons, protons and electrons decrease much faster than for muons.

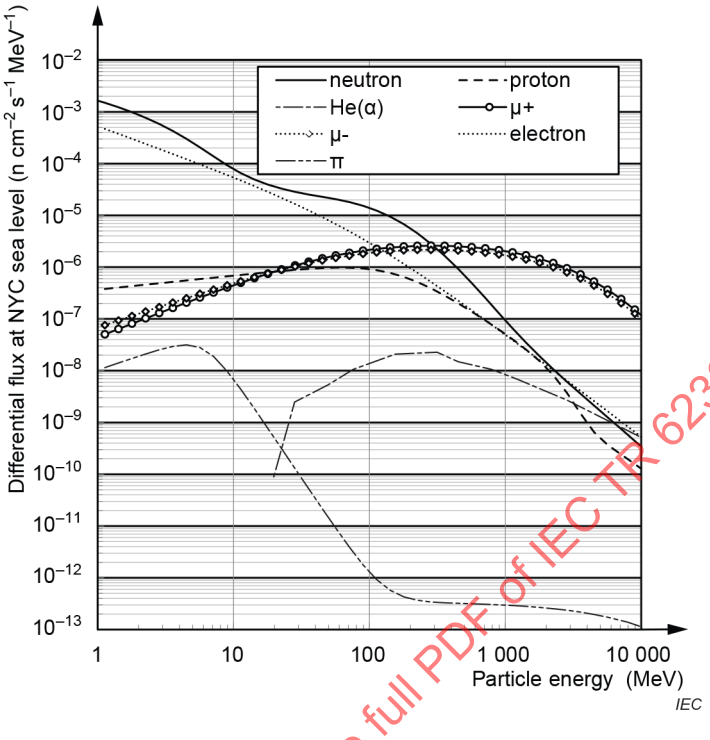

Figure 9 – Differential flux of terrestrial radiation at NYC sea level

Figure 10 summarizes measured neutron spectra in the energy range of thermal neutrons to 100 GeV together with JEDEC JESD89 [2] fitting curve at the ground and avionics level. Neutron flux at avionics altitude is higher than that at the ground by a factor of 10 to 1 000. The factor becomes larger at the higher energy.

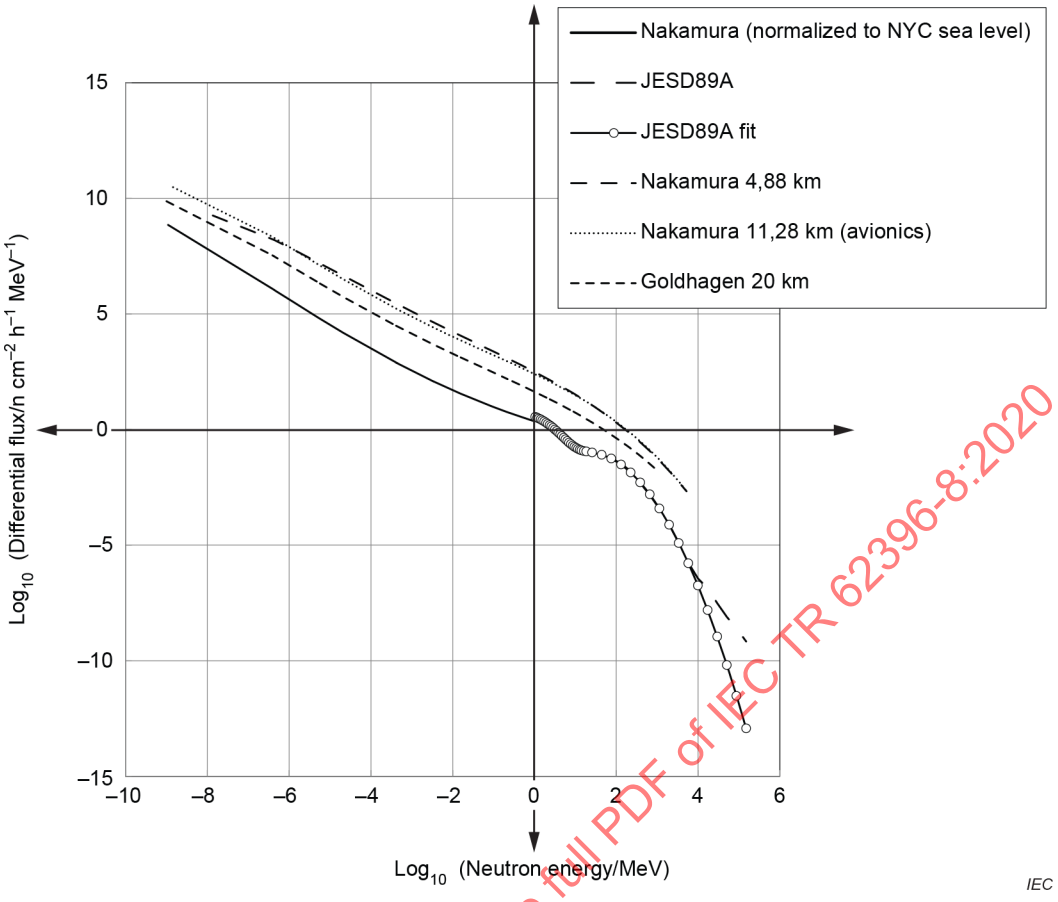

Figure 10 – Measured differential flux of high-energy neutrons at NYC sea level and at avionics altitudes (5 000 m, 11 000 m and 20 000 m)

When looking at the differential flux curve on log-log axes as in Figure 8 to Figure 10, one can feel that the contribution of low-energy neutrons to the total flux is much higher than that of high-energy neutrons. This can cause misunderstanding: the low-energy neutron flux is exaggerated by differentiating in narrow energy bands in the logarithmic scale. In contrast, when cumulative flux above a given particle energy is plotted, as in Figure 11, one can have much clearer images.

Where total flux above a certain energy needs to be known, as it is often the case in SEE evaluation, the cumulative flux plot is useful.

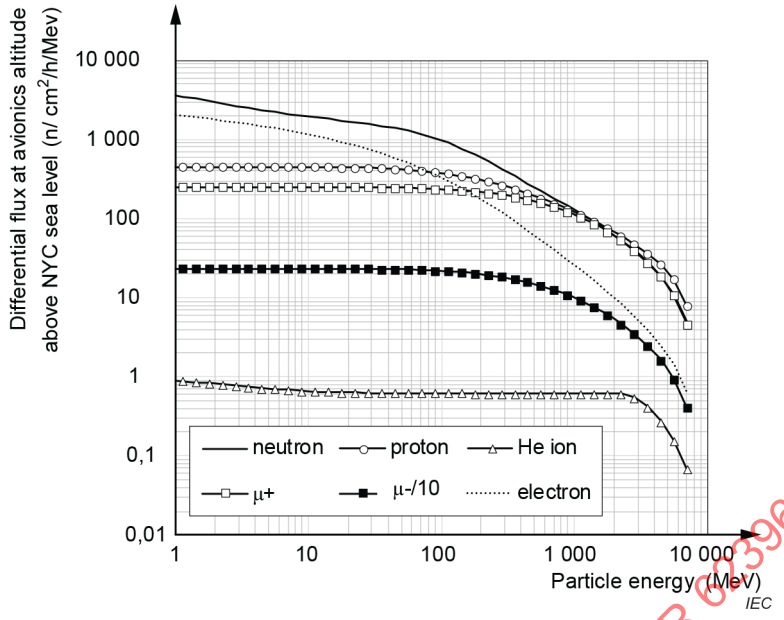

Figure 11 – Cumulative flux of terrestrial radiation at avionics altitude above NYC sea level

4.4 Particle considerations

4.4.1 General

Subclause 4.4 describes SEE test results for the particles of interest, with reference to the literature. Test techniques and facilities are described with relevant references in IEC 62396-1:2016, Annex C.

4.4.2 Alpha particles

Alpha particle SEE tests are normally carried out using alpha-emitting radioisotopes, in particular ^{241}Am, in accordance with IEC 60749-38, JEDEC JESD89 [2, 15], and JEITA EDR-4705 [16]. The motivation for such tests is typically to evaluate soft-error rate susceptibility in the presence of radioactive contaminants contained within a DUT (mainly ^{210}Po, ^{232}Th and ^{238}U). ^{210}Po is mainly contained in solder bumps as an impurity in Pb. ^{232}Th and ^{238}U are mainly contained in package materials.

It is known that the contribution of alpha particles to total soft-error rate in DRAMs becomes negligibly small as device scaling proceeds [3]. While further scaling has caused an increase in neutron soft error in SRAMs, the contribution of alpha-particle soft-errors seems to be increasing mainly due to the decrease in critical charge in SRAMs. Wilkinson *et al.* [17, 18] have made measurements on alpha-ray soft-error in SRAMs, indicating that the proportion of SEE caused by alpha particles has been increasing, albeit with substantial uncertainty in measurements.

Table 4 summarizes properties of alpha-particle sources for accelerated experiments. In some cases, accelerators are used to produce high-energy helium ion beams.

Table 4 – Non-exhaustive list of methods for alpha-particle SEE measurements

Facility	Energy /MeV	LET in Si /MeV·cm^2·mg^{-1}	Flux /α·cm^{-2}·s^{-1}	Note	Ref.
IBM T. J. Watson Laboratory 3 MV tandem accelerator, Yorktown Heights, US-NY	4 to 7		5×10^6	65 nm SOI latch experiment	[19]
	0,6 to 9			32 nm, 45 nm SOI latch experiment	[20]
Cyclotron Institute Texas A&M University (TAMU), College Station US-TX	60, 99	0,11; 0,07 (initial, in vacuum); 1,5 (at Bragg peak)			[21]
^{241}Am		0,7		90 nm, 130 nm, 250 nm SRAM experiment	[22]
				100 µCi	[23]
^{232}Th		0,6		90 nm, 130 nm, 250 nm SRAM experiment	[22]

Some examples of alpha particle analyses from the literature follow.

KleinOsowski *et al*. [19] and Rodbell *et al*. [20] evaluated alpha-particle soft-errors in 65 nm, 45 nm and 32 nm SOI latches using the IBM T. J. Watson Laboratory 3 MeV tandem accelerator. The effects of transistor width/layout and beam angle were evaluated.

Swift [21] utilized the TAMU cyclotron as an alpha particle source. The merit of using accelerators as the alpha-ray sources is that the beam can be collimated and its angle and hit location can be controlled.

Roche *et al.* [22] made alpha-particle soft-error experiments in 250 nm, 130 nm, and 90 nm SOI/bulk SRAMs using ^{241}Am and ^{232}Th sources, demonstrating low susceptibility in SOI SRAMs compared to bulk SRAMs.

Gasiot *et al*. [23] further made ^{241}Am alpha-particle soft-error tests in 130 nm, 90 nm, and 65 nm SRAMs and showed an increase in MCU rate with 65 nm SRAMs partly due to the bipolar effect.

Takasu *et al*. [24] developed a method in which a CR-39 monomer is placed on and exposed to a device in a vacuum chamber and the number of etch pits in the CR-39 monomer created by alpha particles is counted after chemical etching treatments, and demonstrated the detection limit $3{,}2 \times 10^{-5}$ h^{-1}cm^{-2} of an alpha-particle flux, which is well below HLA level (hyper low alpha, 5×10^{-4} h^{-1}cm^{-2}).

4.4.3 Protons

SEE phenomena due to high-energy protons have been studied experimentally by many researchers, often motivated by the need to understand effects in spacecraft due to galactic cosmic rays, solar particles, and trapped radiation. High-energy protons have also been used as proxies for neutrons, as their reactions are similar, with some small differences below about 50 MeV due to Coulomb barrier effects as illustrated by Figure 12 [25, 26]. More recently, it has been observed that SEE is caused by direct ionization from protons at lower energies, and testing at proton energies below 10 MeV has also been done.

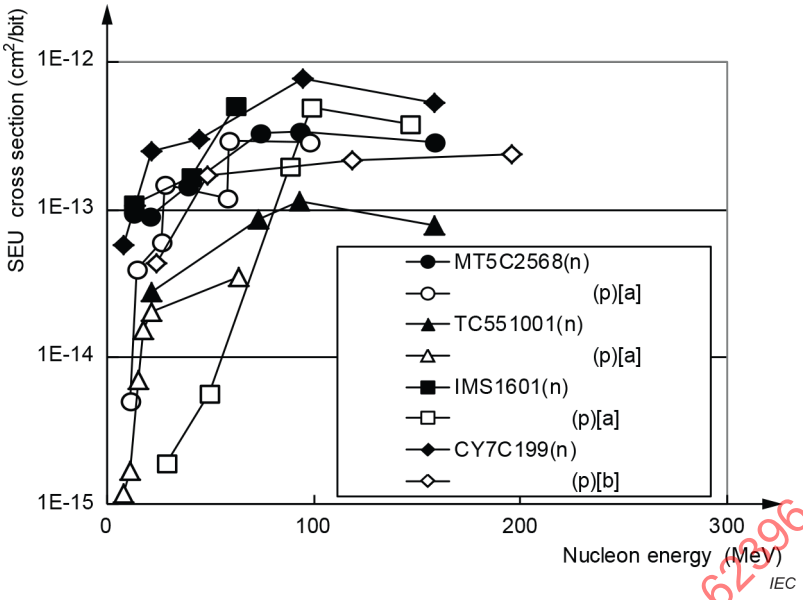

NOTE [a] see [25], [b] see [26].

Figure 12 – Comparison of measured cross section of memory devices irradiated by high-energy protons and neutrons

Table 5 summarizes typical proton accelerator facilities used for terrestrial or cosmic radiation effects (see also IEC 62396-1:2016, Annex C).

Table 5 – Non-exhaustive list of facilities for proton irradiation

Facility	Ref.	Type	Energy /MeV	Flux $p \cdot cm^{-2} \cdot s^{-1}$	Ref.
TRIUMF Proton Irradiation Facility (PIF), Vancouver, CA	[27, 28]	Cyclotron	34,5 to 498	1,44 to $8,52 \times 10^{11}$	[29]
			35,4; 105; 498		[30]
			20 to 498		[31]
			20 to 520	1×10^{5} to 1×10^{8}	[32]
			50; 100; 200; 350; 500		[33]
			20 to 500		[34]
			105		[35]
			13; 20; 35; 63; 101; 194; 348; 490		[36]
The Svedberg Laboratory (TSL) Uppsala, SE		Cyclotron	24; 49; 119; 196		[26]
			21; 46; 88		[37]
Francis H. Burr Proton Therapy Center (formerly Northeast Proton Therapy Center), Boston, US-MA		Cyclotron	10 to 225		[38]
			220	$2,5 \times 10^{8}$	[39]
			150	$8,2 \times 10^{7}$	[40] [41]

Facility	Ref.	Type	Energy /MeV	Flux $p \cdot cm^{-2} \cdot s^{-1}$	Ref.
Indiana University Cyclotron Facility (IUCF) Bloomington, US-IN		Cyclotron	52; 89; 198		[42]
			65; 200		[43]
			50; 100; 150; 200		[44]
			98; 198		[45]
			100; 200		[46]
			27; 198		[47]
Lawrence Berkeley Laboratory (LBL), Berkeley, US-CA	[48]	Cyclotron	1,2; 6; 32		[45]
			0,35; 3; 5		[49]
			0,65; 1; 2	6×10^2 to 5×10^6	[42]
IBM T.J. Watson Research Center, Yorktown Heights, US-NY		Tandem Van de Graaf	0,6 to 6		[50]
UC Davis Crocker Nuclear Lab (CNL) Davis, US-CA	[51]	Cyclotron	19; 8; 2,6		[45]
			8 to 63		[34]
			1,09; 4,47		[47]
Hahn-Meitner Institute, Berlin, DE	[52]	Cyclotron	2; 68		[53]
NASA Goddard Space Flight Center (GSFC), Greenbelt, US-MD		Van de Graaf	<2		[45]

Some examples of proton analyses from the literature follow.

Cellere *et al*. [29] used TRIUMF [27, 28] for proton and heavy ion irradiation tests of NAND flash memories and suggested the effects of recoils from nuclear reaction of protons with tungsten.

Gerardin *et al.* [30] evaluated 41 nm floating gate errors in flash memories using proton beam irradiation at TRIUMF, emphasizing the impact of protons on floating gate errors by direct ionization and spallation reaction.

Shaneyfelt *et al*. [31] utilized TRIUMF, IUCF and LANSCE (see 4.4.6.4) for protons and neutrons.

Hiemstra *et al*. [32] performed proton irradiation tests of Pentium MMX (233 MHz, 350 nm, 4,5 M transistors) and Pentium II processors (333 MHz, 250 nm, 7,5 M transistors) with ECC in L1 and L2 caches at TRIUMF.

Baggio *et al.* [33] made proton SEE measurements at TRIUMF across a wide range of high energies, from 50 MeV to 500 MeV, for comparison with neutron SEE data.

Schwank *et al.* [34] utilized TRIUMF for space application of commercial SRAMs (140 nm to 500 nm).

Rufenacht *et al*. [35] carried out partial irradiation test of an ESP603 single board computer and power 603 microprocessor using a 105 MeV proton beam at TRIUMF. They separated the ESP603 into 8 regions (6 cm × 6 cm each) including DRAMs, FPGAs, clock buffers, EEPROMs, voltage regulator, and examined SEU characteristics in each region.

Dyer, *et al.* [36] measured neutron and proton SEU cross section of 4 Mbit SRAMs by using NPL, TSL, and TRIUMF across a wide range of energies.

Johansson *et al*. [26] and Granlund *et al*. [37] made high-energy proton SEE measurements at TSL for comparison with neutron SEE data.

Liu *et al*. [38] and McMarr *et al*. [39] made proton SEE measurements at the Northeast Proton Therapy Center, with energies in the range of 10 MeV to 225 MeV.

Kellington *et al.* [40] evaluated derating in IBM power6 microprocessor (65 nm SOI process, dual core with on-board L2 and L3 caches) by 150 MeV protons at the same facility, renamed the Francis H. Burr Proton Therapy Center.

Rao *et al*. [41] also evaluated the dependency of SER on workload in IBM power6, Intel Core2 5160, and Xeon Woodcrest Microprocessors by 145 MeV to 150 MeV proton irradiation at the Francis H. Burr Proton Therapy Center.

Lawrence *et al*. [42] evaluated the susceptibility of 90 nm bulk CMOS SRAMs to low-energy protons at LBL and compared results with those from high-energy proton tests at IUCF. Hardened SRAMs (with additional capacitors and resistors) and non-hardened SRAMs were tested. A drastic increase in SEU sensitivity was observed for non-hardened SRAMs below 1 MeV by a factor as high as 5 to 6 orders of magnitude.

Quinn *et al*. [43] measured proton-induced SEU in Xilinx Virtex 5 FPGAs at 65 MeV and 200 MeV IUCF.

Gadlage *et al*. [44] examined operating-frequency effects on SEU cross sections in a pipeline architecture of inverter chains with DICE or unhardened D-flip-flops in between. SEU rate in D-flip-flops is the sum of the contribution by direct hit of protons at sensitive nodes in flip-flops and the contribution by SETs created in the combinational logic circuit (inverter chain) upstream of the flip-flops and captured in the flip-flops. The probability of capture increases as frequency increases so that total SEUs in flip-flops starts to increase at a certain frequency (the "crossover frequency"). They showed a trend approaching to the crossover frequency at about 1 GHz by 200 MeV proton irradiation and about a few hundred megahertz by heavy ion irradiation.

Sierawski *et al*. [45] examined low-energy proton effects on SEU sensitivities in 65 nm SRAMs at GSFC, IUCF, and LBL [48]. They found that the contribution of protons with energy below 2 MeV was higher than those with energy above 100 MeV by more than two orders of magnitude. They attributed this increase in contribution to direct ionization by low-energy protons. Low-energy protons have much larger energy deposition near their Bragg peak energy compared to the critical charge that is decreasing by scaling.

Oldham *et al*. [46] used 100 MeV and 200 MeV protons at IUCF to evaluate radiation effects in commercial 90 nm NAND Flash non-volatile memory.

Seifert *et al*. [47] examined the susceptibility of 45 nm and 32 nm bulk CMOS latches to low-energy protons at IUCF and CNL [51]. They used degraders to reduce proton energies down to below 1 MeV and saw no drastic increase in SEU cross section from 45 nm to 32 nm latches unless operating voltage was reduced.

Puchner *et al.* [49] evaluated the effects of low-energy protons on SEUs in 90 nm and 65 nm SRAMs using the LBNL low-energy proton beam tuned by degrader foils down to 0,35 MeV. They also showed an increase in SEU cross section below 2 MeV, by a factor of two orders of magnitude.

Rodbell *et al.* [50] used the IBM T. J. Watson Laboratory tandem accelerator to investigate the effects of critical charge decrease on SEU characteristics in 65 nm SOI SRAMs and latches. They estimated critical charge from the critical grazing angle of protons at which SEUs took place and obtained values as low as 0,24 fC to 0,27 fC and 0,14 fC to 0,16 fC for SRAMs and latches, respectively. They also emphasized the effects of the metal layer structure on the variation in critical charge.

Sonia *et al.* [53] evaluated proton beam irradiation effects on AlGaN/GaN heterostructure FETs at the Hahn-Meitner Institute, now the Helmholtz Zentrum Berlin [52].

4.4.4 Muons and pions

Muons and pions have potential to cause SEE through direct ionization. Their SEE can be evaluated in a similar manner to the tests with other charged particles. A simplified muon/pion irradiation system is illustrated in Figure 13.

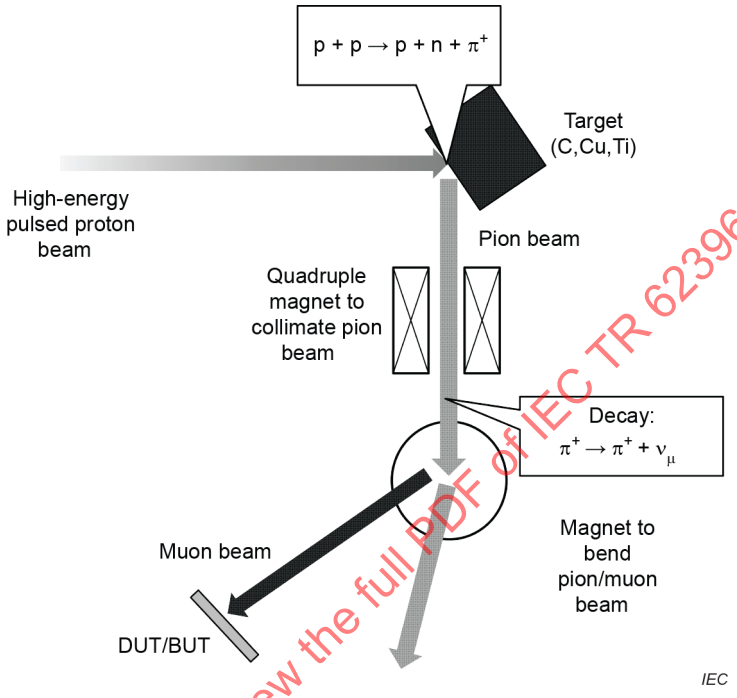

Figure 13 – Simplified scheme of muon/pion irradiation system

Muons can be produced from pions through decay reactions:

$$\pi^- \rightarrow \mu^- + \overline{\nu_\mu}$$
$$\pi^+ \rightarrow \mu^+ + \nu_\mu \quad (3)$$

To produce a positive pion, a high-energy proton with kinetic energy of more than 300 MeV has to collide with a proton in a target nucleus (C, Cu, etc.) with the reaction:

$$p^+ + p^+ \rightarrow p^+ + n^0 + \pi^+ \quad (4)$$

Negative pions can be produced by bombarding high-energy neutrons on the target:

$$n^0 + p^+ \rightarrow p^+ + p^+ + \pi^- \quad (5)$$

or else in the vicinity of a proton-proton collision site where a high-energy neutron produced by reaction (4) can produce a negative pion by reaction (5). The muon beam is separated from the pion beam magnetically.

Artificial production of muons requires a very high-energy proton accelerator and collision/beam transfer equipment such that only a few of these facilities are available or in development worldwide [27, 54, 55, 56, 57, 58], as summarized in Table 6. In most of these, pion beams can be available because pions are intermediate products of muon beam lines as illustrated in Figure 13, although there are only old reports of using LANSCE for this purpose (formerly LAMPF, Los Alamos Meson Physics Facility; the muon test facility is no longer available at LANSCE), as for example the report of Dicello *et al.* [59]. They report that negative pions produced SEU in AM9114 EPS 4 kb SRAMs with a device cross section of 6×10^{-8} cm^{-2}. The corresponding cross section for SEU caused by positive pions was less than 1×10^{-11} cm^{-2}. No error was detected by muon irradiation up to a fluence of 8×10^{10} cm^{-2}. The relative impact of pions on soft-error would have been 10 000 times higher than that of muons if fluences of both particles were the same. In the field, however, the flux of pions is much lower than that of muons so that the impact of pions on SER could be neglected.

Table 6 – Non-exhaustive list of facilities for muon irradiation

Place	Facility Name	Acronym	Primary Ion	Target	Momentum /MeV·c^{-1} (or energy /MeV)	Flux	Note	Ref.
Ibaraki, JP	Japan Proton Accelerator Research Complex	MUSE/ J-PARC	P	C	4 to 55	4×10^{6} s^{-1} (4π)	-	[54]
		PRISM/ J-PARC	50 GeV p		68	1×10^{12} s^{-1} (4π)	Under construction	[55]
Harwell, GB	Rutherford Appleton Laboratory	RIKEN-RAL/ISIS	800 MeV p	C	140 to 240			[56]
		MICE/ ISIS		Ti	20 to 120		Muon ionisation cooling experiment	[57]
Villigen, CH	Paul Scherrer Institut	PSI	500 MeV p		10 to 280	$3{,}0 \times 10^{6}$ s^{-1} (4π)	6 beam lines	[58]
Los Alamos, US-NM	Los Alamos Meson Physics Facility	LAMPF	800 MeV p	C	109	5×10^{4} cm^{-2}·s^{-1}	Pion beam with momentum 164 MeV·c^{-1} and flux $1{,}6 \times 10^{6}$ cm^{-2}·s^{-1} is available	[59]
Vancouver, CA	TRIUMF	M20B/ TRIUMF	500 MeV p	Be	20 to 200	$1{,}4 \times 10^{6}$ s^{-1} (4π)	6 beam lines	[60]

Sierawski *et al.* [60] demonstrated that low-energy muons, in particular antimuons (μ^+), can cause SEU in 65 nm, 45 nm, and 40 nm SRAMs. They used muon beam line M20B at TRIUMF with an estimated SEU cross section of 1×10^{-13} cm^{-2}·bit^{-1} at the energy of around 0,3 MeV to 0,8 MeV. They concluded that soft error induced by terrestrial muons is not substantial for current generation compared to the contribution of neutrons, but can have an impact when the critical charge decreases with silicon feature size scaling.

Ibe *et al.* [61] evaluated the total upper bound charge collection by sea-level muons based on simulated muon spectrum and showed a possible impact larger than that of neutrons can be observed when critical charge is below 1 fC.

The impact of muons on SEE in electronic devices manufactured with 28 nm to 40 nm silicon feature sizes is reportedly not so significant, demonstrated by μ^+ beam experiments [62, 63], but can pose a certain threat for very small silicon feature sizes below 20 nm.

4.4.5 Low-energy neutrons

Low-energy neutrons can cause SEE by interaction with boron-10, as shown conclusively by Baumann *et al*. [64]. Boron-10 reacts very strongly with low-energy neutrons, releasing a lithium ion and an alpha particle with total ionizing energy up to 2,8 MeV. Boron-10 was formerly routinely used in commercial electronics as a constituent of BPSG films used for planarization. Even where boron-10 is no longer used for this purpose, more recent technologies have also shown susceptibility to SEE from low-energy neutrons due to the presence of boron-10 [65, 66] apparently associated with etchants used in the deposition of metal layers [67].

Thermal neutrons are those in thermal equilibrium with their surroundings, nominally at 25 meV at 300 K, and sometimes defined loosely as those with energy less than 1 eV. Epithermal neutrons are those at slightly higher energies, nominally in the range from 1 eV to 10 keV. Epithermal and thermal neutrons that appear in atmospheric radiation field as neutrons originally generated at high energies lose energy by scattering off materials in the environment. Thermal and epithermal flux is therefore highly dependent on the environment.

Thermal neutrons can be obtained in experimental nuclear fission reactor where neutrons in the reactor core are in thermal equilibrium with water coolant acting as a moderator [68, 69]. Thermal and/or epi-thermal neutrons can also be obtained from accelerator sources by moderating a fast neutron beam in the same way [27, 28]. Cold neutrons are those at lower energies, from a distribution in equilibrium with a cryogenic moderator.

In neutron beams with mixed thermal and high-energy components, thermal neutrons can be shielded against by wrapping DUTs with cadmium sheets, which are readily available. SEE tests with and without such wrapping make the effect of thermal neutrons clear. The cross section of cadmium to low-energy neutrons is shown in Figure 14, which shows how cadmium effectively filters neutrons with energy below approximately 1 eV.

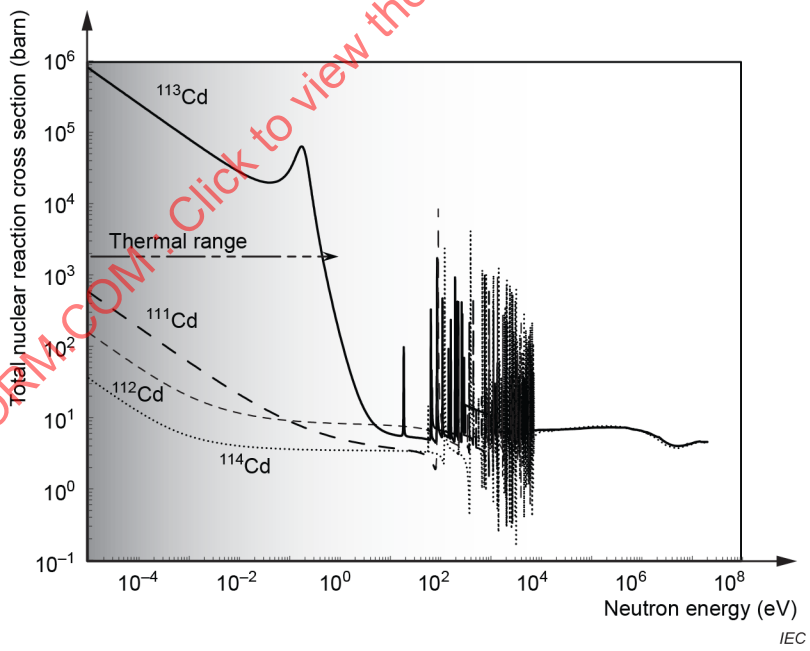

Figure 14 – Nuclear capture of cross section of cadmium isotopes

Some irradiation facilities where low-energy neutrons are available are listed in Table 7.

Table 7 – Non-exhaustive list of facilities for thermal/epi-thermal neutron irradiation

Place	Facility name	Acronym	Source	Energy	Flux /n·cm^2·s^{-1}	Note	Ref.
Gaithersburg, MD	Cold Neutron Research Facility (NIST)	CNRF	Heavy water nuclear rector	Cold (20 K)	6,29 × 10^8	NG0 beam line was used	[64]
Boston, MA	Nuclear Reactor Laboratory	MITR	Nuclear fission reactor	Thermal-epithermal	Epithermal 5 × 10^9 Thermal <1 × 10^{10}	For BCNT	[68]
Osaka, Japan	Kyoto University Research Reactor Institute	KUR	Heavy water nuclear rector	Thermal, 24 keV	3,9 × 10^{12} to 28 × 10^{12} 6,8 × 10^6 at 24 keV	-	[69]
Vancouver, Canada	Thermal Neutron Facility	TRIUMF	Cyclotron (500 MeV proton)	Thermal	1 × 10^{12}	Epithermal beam is also available	[70]
Ibaraki, Japan	Japan Proton Accelerator Research Complex	J-PARC	Hg(p,n)	10^{-4} eV to 0,1 eV (after attenuation)	0,1 × 10^8 to 4,6 × 10^8	-	[71]

Some examples of low-energy neutron analyses from the literature follow.

Baumann *et al*. [64] were the first to show that ^{10}B in BPSG film, which can be used for smoothing the surface of semiconductor wafer for precise lithography, is responsible for thermal neutron induced soft-error by the neutron capture reaction, n + ^{10}B → α + ^{7}Li. They used cold neutrons in equilibrium with a 20 K (−253 °C) environment at the NG0 beam line in CNRF, NIST, for SEU measurement of SRAMs, and confirmed the impact of thermal neutrons by comparing the number of soft-errors with and without a BPSG layer. A BF_3 thermal neutron counter utilizes the same capture reaction as the detection mechanism and so the calibration is reportedly easy.

Dyer *et al*. [70] made thermal neutron measurements at IUCF/LENS, TRIUMF, NIST and NPL and compared with high-energy neutron test data of SRAMs at LANSCE, TSL, and TRIUMF.

Zhang *et al*. [71] evaluated thermal neutron induced soft-errors in 32 nm HKMG SRAMs using two thermal neutron facilities. They concluded that thermal neutrons do not cause MBU/SEFI/SEL in 32 nm HKMG SRAMs and they pointed out the importance of accurate measurement of flux, calculation of effective flux and shielding effects of package materials.

4.4.6 High-energy neutrons

4.4.6.1 General

High-energy neutrons can cause SEE through nuclear reactions with electronic device materials. A range of techniques are available for generating high-energy neutrons for test purposes, and it is convenient to divide them into those with maximum energies below 20 MeV and those with maximum energies above 20 MeV.

Below 20MeV two kinds of sources are available. Radioisotope sources provide neutrons with a wide range of energies below about 10 MeV. Accelerator sources can provide monoenergetic neutrons with energies in the range from about 1 MeV to about 15 MeV.

Above 20 MeV there are no monoenergetic neutron sources available; but quasi-monoenergetic sources can be used to provide a neutron spectrum strongly peaked at a nominal energy determined by a proton energy delivered by a particle accelerator and with a significant tail of neutrons at lower energies. Finally, spallation neutron sources provide broad spectra up to a maximum determined by the energy of an initiating proton delivered by a particle accelerator. Neutron spectra in spallation sources can approximate the neutron spectrum in the atmospheric radiation environment.

4.4.6.2 High-energy neutrons with energies limited to below 20 MeV

Monoenergetic neutrons in the range from 1 MeV to 15 MeV can be produced by P-T (proton-tritium), D-D (deuterium-deuterium) and D-T (deuterium-tritium) reactions. When an accelerated particle X collides with a target nucleus y, producing light particle ω and residual nucleus Z, this reaction can be expressed in the following form:

$$\mathrm{X}(\mathrm{y},\omega)\mathrm{Z} \tag{6}$$

The difference in static total mass $(m_X+m_y)c^2$ of reactants (X and y) and $(m_\omega+m_Z)\,c^2$ of products (ω and Z) is called the Q-value and is defined by:

$$Q=\left(m_X+m_y\right)c^2-\left(m_\omega+m_Z\right)c^2 \tag{7}$$

There are some calculation tools of the Q values at the website [72].

The P-T, D-D, and D-T reactions to produce neutrons can be expressed as follows in the case of the Fast Neutron Laboratory (FNL), Tohoku University:

T(p,n)3He (Q value = -0,7638 MeV, En = 1 and 2 MeV) (8)

D(d,n)3He (3,2689 MeV, En = 5 MeV); (9)

T(d,n)4He (17,589 MeV, En = 15 MeV). (10)

When the Q value is positive as in the case of Formulae (9) and (10), the reaction is exothermic and only the kinetic energy of particle X necessary to contact with the target is necessary to promote the reaction. When the Q value is negative as in the case of Formula (8), the reaction is endothermic and the particle X needs to be accelerated to have kinetic energy above the Q value in order to trigger the reaction.

Actual neutron spectra at FNL are monoenergetic and shown in Figure 15.

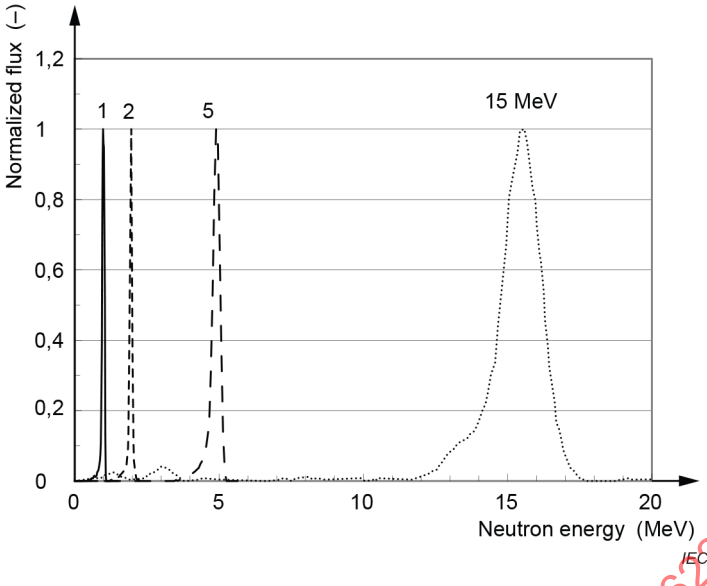

Figure 15 – Neutron energy spectra of monoenergetic neutron beam facilities

Neutrons with energies up to about 10 MeV can be obtained by using radioisotopes such as ^{241}Am-^{9}Be, ^{239}Pu-^{9}Be and ^{252}Cf. ^{241}Am-Be and ^{239}Pu-Be neutron sources contain the alpha-particle emitters ^{241}Am and ^{239}Pu and exploit the nuclear reaction ^{9}Be(α,n)^{12}C. ^{252}Cf decays by spontaneous fission reaction to produce neutrons.

Typical neutron spectra from these neutron sources are shown in Figure 16. ^{252}Cf has a single peak around 1 MeV, while ^{241}Am-Be and ^{239}Pu-Be sources have several peaks in the range from 2 MeV to 10 MeV.

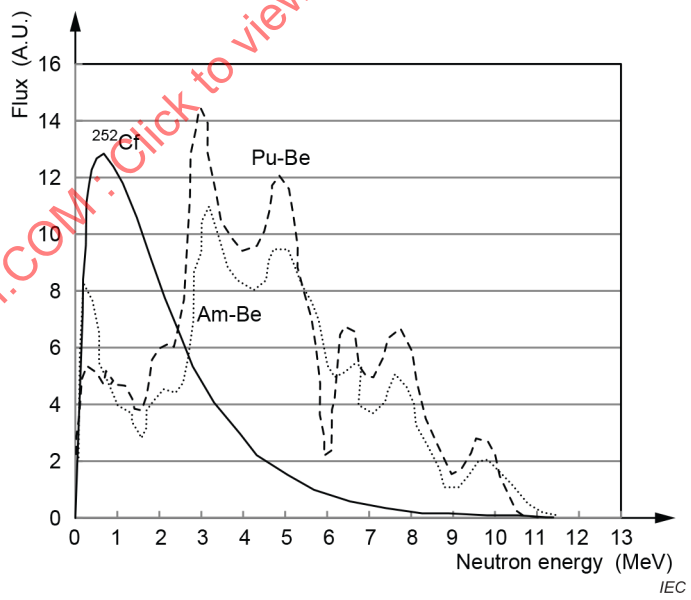

Figure 16 – Neutron energy spectra from radioisotope neutron sources

Table 8 summarizes facilities where a medium energy neutron beam is available by using radioisotopes or accelerators.

Table 8 – Non-exhaustive list of facilities for low-energy neutron irradiation

Place	Facility name	Acronym	Source	Energy /MeV	Flux /n·cm^{2}·s^{-1}	Note	Ref.
Sendai, JP	Fast Neutron Laboratory, Tohoku University	FNL	T(p,n)^{3}He D(d,n)^{3}He T(d,n)^{4}He	1, 2, 5, 15	1,2 × 10^{5} to 9 × 10^{5} at 10 cm from the target centre		[3] [73]
Bloomington, US-IN	Low-energy Neutron Source	IUCF/LENS	Be(p,n)B	3 to 5		200 MeV proton from the IU cyclotron is used	[70]
Essone, FR	Bruyères le Châtel	CEA/DIF	D(d,n)^{3}He	2,5, 4, 6	3 × 10^{4}	4 MV van de Graaf	[33]
Dijon, FR	Valdun Centre for Nuclear Studies	CEA/CVA	T(d,n)^{4}He	14	1 × 10^{9} 1 × 10^{11} (4π)	SAMES accelerator	[33] [74]
Teddington, GB	National Physical Laboratory	NPL	T(d,n)^{4}He	14,5			[70]
Bloomington, US-IN	Indiana University Cyclotron Facility	IUCF	Pu-Be	1 to 11			[75]
Ibaraki, JP	National Metrology Institute of Japan	NMIJ	Be(α,n)^{12}C Li(p,n)^{7}Be	5, 8	10^{11} to 10^{15}	Proton and alpha particles are from the pelletron accelerator	[76]
			D(d,n)^{3}He	2,5, 14,8	10^{11} to 10^{15}	Cockroft-Walton accelerator	
Grenoble, FR	Laboratoire de Physique Subatomique et de Cosmologie	LPSC					[77]

Some examples of neutron analyses from the literature follow.

Savage *et al.* [75] used ^{239}Pu-Be neutron source at IUCF together with proton beam irradiation to evaluate an Omni Wave 256 kb SRAM that was known to have very high sensitivity to soft-errors. Angular dependency of neutron induced soft-error was reportedly observed and attributed to knock-on collision of hydrogen (proton) contained in the device and direct ionization by protons.

At the NMIJ, in addition to ^{7}Li(p,n)^{7}Be and D(d,n)^{3}He reactions, the ^{9}Be(α,n)^{12}C reaction is exploited to produce 5 MeV and 8 MeV monoenergetic neutrons [76].

Yahagi *et al.* were the first to point out the importance of 1 MeV to 5 MeV range neutrons to CMOS SRAM soft-error by using FNL [73].

Dyer *et al.* [70] evaluated the SEE sensitivity of CMOS SRAMs in a wide energy range (thermal to 800 MeV) of neutrons by using various facilities such as TRIUMF (thermal), LENS (3 MeV to 5 MeV), TSL (20 MeV to 180 MeV), TRIUMF (500 MeV) and LANSCE (800 MeV).

Baggio *et al.* [33] evaluated SEE in partially depleted (PD) and fully depleted (FD) SOI devices for neutrons at 2,5 MeV, 4 MeV, 6 MeV, and 14 MeV. They found that body ties reduced SEU cross section by a factor of 100 and that their PDSOI devices had relatively high sensitivity to low-energy neutrons.

Gasiot *et al*. [74] evaluated the sensitivity of 250 nm bulk and SOI SRAMs to 14 MeV neutrons at CEA/CVA, including angle dependency.

Miller *et al.* [77] investigated the capabilities of 14 MeV neutron tests to characterize the single event upset sensitivity of digital devices.

4.4.6.3 High-energy neutrons with energies extending above 20 MeV

A quasi-monoenergetic (QMN) neutron beam can be obtained by bombarding high-energy protons onto a thin target plate typically made of lithium. A simplified setup for a QMN facility is shown in Figure 17.

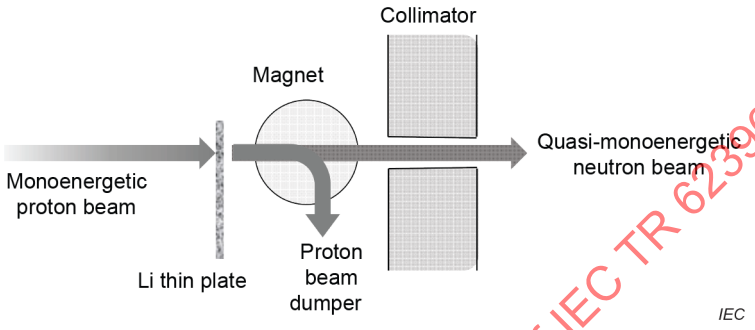

Figure 17 – Simplified high-energy neutron beam source in a quasi-monoenergetic neutron source

Neutrons are produced under the following reaction:

$$p(^7Li,n)^7Be \quad (11)$$

This reaction is a knock-on collision of an incident proton and a neutron in the target nucleus such that the kinetic energy of the neutron is almost the same as that of the proton. Since proton and target nuclei have positive charge, the kinetic energy of the proton and thus the kinetic energy of the released neutron are reduced by the Coulomb barrier energy, E_C:

$$E_C = \frac{e^2}{4\pi\varepsilon_0} \times \frac{Z_I Z_T}{r_I + r_T} = 1{,}438 \times \frac{Z_I Z_T}{r_I + r_T} \quad \text{(MeV)} \quad (12)$$

where

ε_0 is the dielectric constant of vacuum;

Z_I is the atomic number of the incident particle;

Z_T is the atomic number of the target nucleus;

r_I is the radius of the incident particle (fm);

r_T is the radius of the target nucleus (fm).

When the incident particle is a proton (Z_I = 1, r_I = 1,2 fm) and the target nucleus is Li (Z_T = 3, r_T= 1,55 fm), Formula (12) gives E_C = 1,57 MeV. Thus, a neutron knocked out by a proton has kinetic energy slightly lower than that of the incident proton.

Figure 18 shows representative QMN spectra. The strong peak at the nominal neutron energy is visible in each case, as is the low-energy neutron tail that distinguishes quasi-monoenergetic spectra from their monoenergetic counterparts discussed in 4.4.6.2.

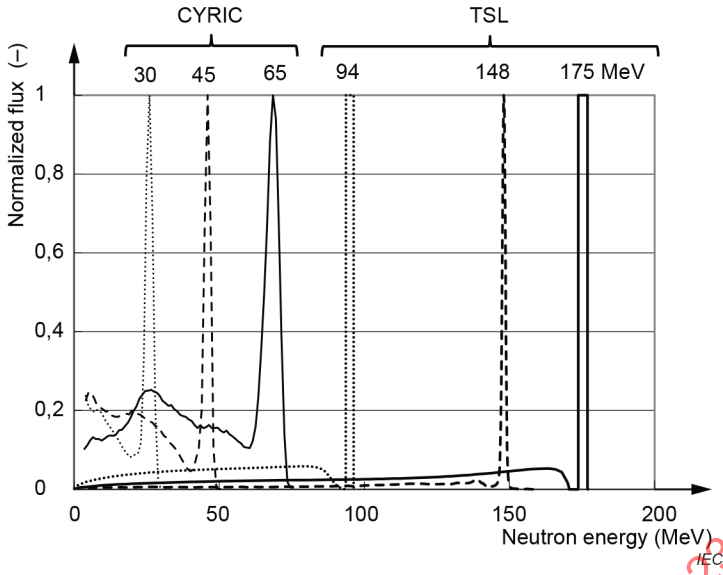

Figure 18 – Neutron energy spectra of quasi-monoenergetic neutron beam facilities

The SEU cross section σ_{SEE} for the peak flux contribution is defined and obtained by:

$$\sigma_{SEE} = \frac{N_{peak\ event}}{\Phi_{peak}} = \frac{R_{peak\ event}}{\phi_{peak}} = \frac{N_{total\ event}}{\Phi_{total}} \times C_{peak} \tag{13}$$

where

$N_{peak\ event}$ is the number of events caused by neutrons in the peak flux area (errors);

Φ_{peak} is the fluence in the peak flux area (n·cm^{-2});

$R_{peak\ event}$ is the single event rate caused by neutrons in the peak flux area (errors h^{-1});

ϕ_{peak} is the flux in the peak flux area (n·cm^{-2}·h^{-1});

$N_{total\ event}$ is the number of events caused by total neutrons (errors);

Φ_{total} is the total neutron fluence (n·cm^{-2});

C_{peak} is a tail correction factor.

The tail correction factor eliminates the contribution of the tail to the total number of events and can be obtained either by unfolding experimental data obtained for several (at least four) different energy peaks [37] or soft-error simulator such as CORIMS [78].

The SEU cross section $\sigma_{SEE}(E_n)$ is thus measured as a function of the neutron energy. The measured data can be approximated by the Weibull fit function:

$$\sigma_{SEE}(E_n) = \sigma_\infty \left[1 - \exp\left\{-\left(\frac{E_n - E_{th}}{W}\right)^S\right\}\right] \tag{14}$$

where

σ_∞ is a saturation value of SEU cross section at high-energy (cm^2);

E_n is the neutron energy at the flux maximum (MeV);

E_{th} is a threshold energy below which σ_{SEE} is zero (MeV);

W is a width factor (MeV);

S is a dimensionless shape factor.

A typical example of this type of curve is shown in Figure 19.

The curve starts from E_{th} and increases gradually to the saturation value σ_∞. SEE rates can be estimated for any neutron spectra including the atmospheric neutron spectrum. SEE rates in any location on Earth, for example, can be obtained from integration of the Weibull fit and differential flux over the energy range from E_{th}:

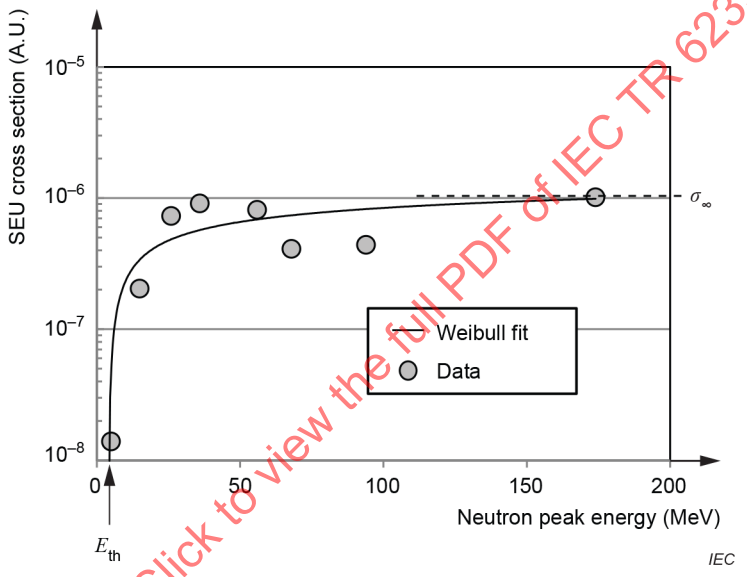

Figure 19 – Conceptual illustration of cross section data obtained by (quasi-) monoenergetic neutron sources and fitting curve by Weibull fit

$$FIT = 10^9 \times \int_{E_{th}}^{\infty} \sigma_{SEE}(E_n) \frac{\partial \phi(E_n)}{\partial E_n} dE_n \quad (15)$$

where

FIT is the single SEE FIT rate;

$\phi(E_n)$ is the neutron flux ($n \cdot cm^{-2} \cdot h^{-1}$).

Some irradiation facilities where quasi-monoenergetic neutrons are available are listed in Table 9.

Table 9 – Non-exhaustive list of facilities for quasi-monoenergetic neutron irradiation

Acronym	Facility name	Place	Source	Energy /MeV	Flux /n·cm^{2}·s^{-1}	Note	Ref.
TSL	The Svedberg Laboratory	Uppsala, Sweden	Li(p,n)^{7}Be	20 to 176	3 × 10^{3} to 3 × 10^{5}	Beam size 1 cm to 80 cm diameter	[26] [73] [79] [80] [37] [36]
CYRIC	Cyclotron and Radio Isotope Center, Tohoku University	Sendai, Japan	Li(p,n)^{7}Be	35 to 65	3 × 10^{5} at 65 MeV	Beam size 10 cm^{2} × 10 cm^{2}	[73] [81] [82]
RCNP	Research Center for Nuclear Physics, Osaka University	Osaka, Japan	Li(p,n)^{7}Be	14 to 198	3 × 10^{3} to 2 × 10^{4}	Beam size 10,8 cm diameter	[83]

Some examples of QMN analyses from the literature follow.

Johansson *et al.* [26] were the first to apply a QMN beam to a SEE test of memory devices and to compare the test results with those by proton beam tests. Substantial differences were observed between quasi-mono-energetic and proton beam tests with almost the same particle energies.

Ibe *et al.* established the QMN test method as the standard test method of semiconductor memory devices using FNL, CYRIC, and TSL [73, 78, 79]. Although high-energy protons were used for SEE tests as proxies for high-energy neutrons, data obtained for the same device with neutrons and protons were not always consistent. In many cases, devices showed different sensitivities between protons and neutrons.

Granlund and Olsson [37] carried out 250 nm to 130 nm SRAM SEU tests using quasi-monoenergetic neutrons at TSL and compared results with those from protons at TSL and spallation neutrons at LANSCE. They observed that SEU cross sections by proton irradiation had higher values by about × 1,9 than for neutrons at energy of 46 MeV regardless of the SRAM part.

Yamamoto *et al*. [83] utilized RCNP as a quasi-monoenergetic neutron source to measure neutron-induced SEU cross section of 180 nm, 150 nm and 130 nm SRAMs and FFs. They fabricated a matrix of FFs similar to an SRAM matrix and demonstrated that the SEU cross sections of FFs were already comparable to those of SRAMs.

Ibe *et al*. [79] were the first to find the bipolar-mode soft-error, MCBI, in 130 nm CMOS SRAMs by using the QMN method. They were also the first to demonstrate that soft errors in memory devices can be basically overwhelmed by applying both interleaving techniques and ECC even for MCBI based on their topological natures: MCUs spread along the bit line (well) and only one- or two-bit-width along the word line (across the well). A drastic decrease in MCUs is reported near p-well taps but this is not true for SBUs, and different SEU mechanisms are implicated between SBUs and MCUs. This observation is supported by Gasiot *et al*. [84] and Nakauchi *et al*. [85] for 65 nm CMOS SRAMs.

Radaelli *et al*. [80] demonstrated a high MCU ratio in 150 nm SRAMs using TSL with peak energies 22 MeV, 47 MeV, 95 MeV, and 144 MeV. The MCU ratio increased with the peak energy. The same observation of the topological nature in MCUs was reported as in [79]. MCUs reportedly decrease only in the bits adjacent to p-well taps.

Shimbo *et al.* [81] applied the partial neutron irradiation method to the test of 90 nm router boards at CYRIC. FPGA, CPU, and SRAM devices were irradiated separately and the SRAM device was identified as the most vulnerable part. SRAMs that did not need speed were replaced by DRAMs with ECC and the total failure rate in the board was reduced by a factor of 9 to 10.

Uezono *et al*. [82] evaluated failure behaviour of ECUs (electronic control units) in automobiles with a variety of workloads by high-energy neutron irradiation tests at CYRIC and ANITA. Consistent results were obtained in test results at both facilities.

4.4.6.4 Spallation neutron consideration

SEE rates also were estimated using spallation neutron sources. A simplified setup for a spallation neutron facility is shown in Figure 20.

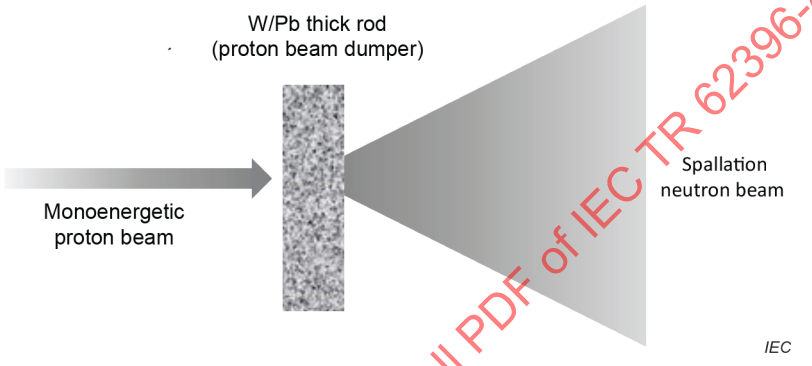

Figure 20 – Simplified high-energy neutron beam source in a spallation neutron source

A spallation neutron source uses a high-energy proton beam to bombard a thick target typically made of tungsten or lead. The spectrum is broad and can mimic the atmospheric neutron spectrum as shown in Figure 21.

Neutron SEE tests using spallation sources are more straightforward than monoenergetic or QMN sources, because the spallation beam more closely mimics the atmospheric neutron environment. SEE rate in service can be predicted by means of a simple acceleration factor.

The measured cross section is:

$$\sigma_{\mathrm{SEE}} = \frac{N_{\mathrm{SEE}}}{\Phi\left(E_{\mathrm{min}}\right)} \tag{16}$$

where N_{SEE} is the number of errors observed during test, and Φ is the measured neutron fluence above a minimum energy.

The predicted error rate in service is then

$$R = \sigma_{\mathrm{SEE}}\phi\left(E_{\mathrm{min}}\right) \tag{17}$$

where ϕ is the in-service fluence rate (flux) above E_{min}.

IEC 62396-1 recommends that E_{min} be 1 MeV for device technologies with silicon feature sizes below 100 nm and can be 10 MeV for larger technologies. If E_{min} is 1 MeV, ϕ is 9,2 × 10^3 n·cm^{-2}·h^{-1}. If E_{min} is 10 MeV, ϕ is 6 × 10^3 n·cm^{-2}·h^{-1}.

This approach is accurate so long as the maximum spallation neutron energy, limited by the incident proton energy, is sufficiently high. An approach to quantifying the fidelity of spallation beams is described in [86] and has been applied to several such facilities [87].

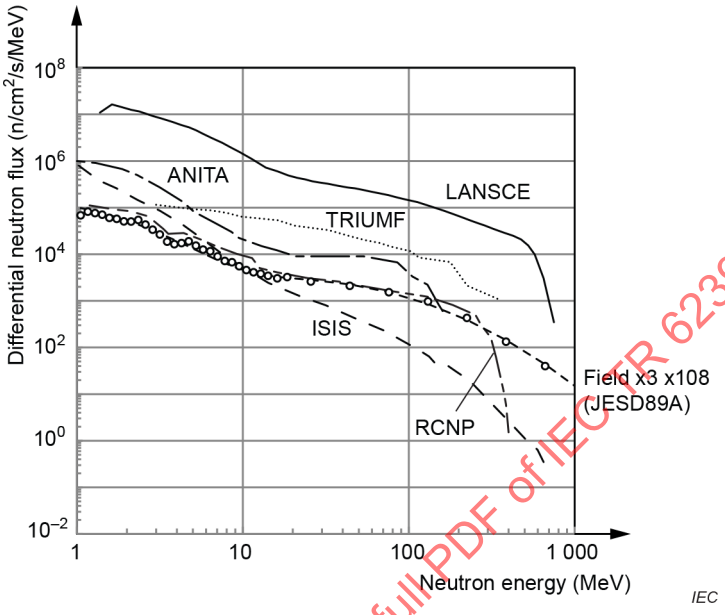

Figure 21 – Neutron energy spectra of spallation neutron sources and terrestrial field

The number of spallation neutron sources available worldwide has increased in recent years. In addition to well-established facilities at LANSCE [88] and TRIUMF [28, 89], facilities at TSL [90], ISIS [91, 92], RCNP [83], and J-PARC [93], among others, have become available. The properties of these sources are summarized in Table 10 (see also IEC 62396-1:2016, Annex C).

Table 10 – Non-exhaustive list of facilities for nuclear spallation neutron irradiation

Acronym	Facility name	Place	Source	Energy /MeV	Flux /n·cm^2·s^{-1}	Note	Ref.
LANSCE	Los Alamos Neutron Science Center	Los Alamos, US-NM	p→W	800	3 × 10^5 (> 1 MeV)	Beam size 8 cm, 5 cm, 2.5 cm	[70] [84] [94]
TRIUMF	TRIUMF	Vancouver, CAa	p→Al p→Pb	450	3 × 10^6 (> 10 MeV)	Beam size 5 cm × 12 cm	[89, 28, 70]
ANITA/TSL	Atmospheric-like neutron from thick target/The Svedberg Laboratory	Uppsala, SE	p→W	180	> × 10^6 (> 1 MeV)	Beam size 1 cm to 80 cm diameter	[90, 95, 82]
ISIS	Rutherford Appleton Laboratory	Harwell, GB	p→W	800	10^5 to 10^7 (collimated) 10^3 to 10^5 (broadened)	Thermal neutrons are also available	[91, 92, 96]
RCNP	Research Center for Nuclear Physics, Osaka University	Osaka, JP	p→W	400	5 × 10^5 (> 10 MeV)	Beam size 10,8 cm diameter	[85, 97, 98, 94]
MLF/J-PARC	Materials and Life-science Facility	Ibaraki, JP	p→Hg	400	-	-	[93]

Some examples of analyses from the literature follow.

Hubert *et al.* [95] used ANITA to demonstrate mitigation techniques of SEUs in content addressable memories (CAMs).

Rech *et al.* [96] demonstrated high susceptibility of GPUs that are used not only in graphic media but also high-end computing and safety critical graphic processing in automobiles. They used ISIS for irradiation tests.

Nakauchi *et al.* [85] evaluated the parasitic bipolar-mode soft-error as introduced in [79] using RCNP and demonstrated a mitigation technique of MCUs by back-bias.

Furuta *et al.* [97] evaluated bipolar-mode soft-error in 65 nm FFs by using RCNP. They found that the dependence of MCU on the tap location seems different from that in SRAMs. The MCU rate was higher in FFs further from tap locations.

Uemura *et al.* [98] also used RCNP to investigate mitigation techniques of FFs, in particular, on MNT in redundancy nodes in DICE-type hardened FFs.

Nishida *et al.* [99, 94] used LANSCE and RCNP to evaluate SEB in IGBTs for automobiles.

4.5 Conclusion and guidelines

Neutrons remain by far the most significant SEE threat to avionics electronic equipment. They are the most prevalent component of the atmospheric radiation field at almost all geomagnetic locations, altitudes, and particle energies. They are highly penetrating and can reach electronic components in aircraft, where they can interact with the nuclei of constituent materials of electronic devices, releasing ionizing energy which can lead to SEE.

High-energy neutrons, above about 1 MeV, can deliver part of their kinetic energy to ionizing particles in interaction with materials of any type. In principle, electronic devices of all kinds and technologies are susceptible to SEE caused by high-energy neutrons.

Low-energy neutrons, at thermal or epithermal energies, can interact with ^{10}B when it is present in a device structure, releasing up to 2,8 MeV of ionizing energy. High-energy neutrons from the atmospheric radiation environment can lose energy and become thermalized as they scatter off aircraft materials, modifying the neutron spectrum and creating a double-sided threat within the aircraft. The thermal and epithermal neutron field within an aircraft is complex and difficult to predict, but components containing ^{10}B are liable to experience SEE due to this environment. Only the ^{10}B isotope is implicated; in modern components this isotope is understood normally to be present only in electronic device overlayers. Historically, ^{10}B has mostly been found in BPSG. Even where BPSG is not used, however, some modern devices have been found to be susceptible to SEE caused by thermal neutron interactions; this is likely to be due to the presence of boron contaminants left over from etching metal overlayers. High-density SRAMS and certain FPGA devices, in particular, have been found to suffer such effects.

Protons can also cause SEE. High-energy protons, at energies above a few megaelectronvolts, can cause interactions in the same way as high-energy neutrons, with little difference in cross section. However, the flux of protons available to cause such an interaction is much lower than the corresponding flux of neutrons. For example, calculations for typical avionics conditions (40 000 ft altitude, 45° latitude, 0° longitude, solar minimum), made with EXPACS 4.02 show that the integral proton flux above 10 MeV is less than 5 % of the corresponding neutron flux.

Nuclear reactions from neutrons and high-energy protons are capable of causing the most damaging SEE phenomena, because they can create highly ionizing particles directly within a device. Directly ionizing particles in the atmospheric radiation spectrum, including alpha particles, low-energy protons, muons, pions, and electrons, have less ionizing power and therefore can only cause a subset of the SEE phenomena that can be caused by neutrons and high-energy protons. Therefore, the kinds of SEE that can be observed from low-energy protons, muons, etc., are the same kinds as can be observed from neutrons, and the same mitigation techniques can be employed.

The rates of SEE than can be caused by low-energy protons, muons, etc., are dependent also on the flux and spectrum of each particle type.

Low-energy protons have been shown to cause SEE in some sensitive electronic device technologies, including SRAMs below 90 nm silicon feature size. Here, "low-energy" means that the proton has sufficient stopping power that it can stop in sensitive volumes or close to sensitive volumes of an electronic device. This does not correspond directly to the low-energy portion of the atmospheric radiation environment, as charged particles slow down as they traverse materials shielding a component, for example an aircraft structure. The quantity of concern here is the particle range, which can be expressed in metres, dependent heavily on the details of a structure being traversed (materials and geometry), or in areal density ($g \cdot cm^{-2}$), which is largely independent of material. For example, protons with energies in the order of 100 MeV have a range of a few centimetres in typical aircraft materials with moderate density.

Muons and pions are capable of causing SEE. Of these particles, the most prevalent in the atmosphere are muons. SEE has been observed due to direct ionization by stopping muons in technologies below 65 nm silicon feature size but is not expected to have a significant effect for technologies above 20 nm silicon feature size. In addition, atmospheric muons are highly penetrating and the number that are likely to stop in avionic components is unlikely to be significant compared to the influence of other atmospheric radiation particles, notably protons and neutrons.

Electrons and positrons are not expected to be significant for SEEs even for very small silicon feature sizes below 20 nm.

Although alpha particles are well known to cause SEE as a result of radioactive decay of package contaminants, there are very few alpha particles in the atmospheric radiation field that are capable of penetrating to active regions of avionic components, and their effect is negligible.

Annex A
(informative)

CMOS semiconductor devices

CMOS devices like SRAMs or FFs are basically made on the stripe structure of p and n dual wells. For example, Figure A.1 shows typical layouts of diffusion layers (nodes) in a one-bit SRAM and an OR gate cell on the stripe structure. All nodes in memories and logic circuits are basically made on the same stripe structure in a device. Unlike dual-well structures, triple-well structures have a deep n-well. As for SOIs, BOXs are made under the dual wells. Isolation oxides, usually shallow STI oxides, are also made to isolate each node in a lateral direction.

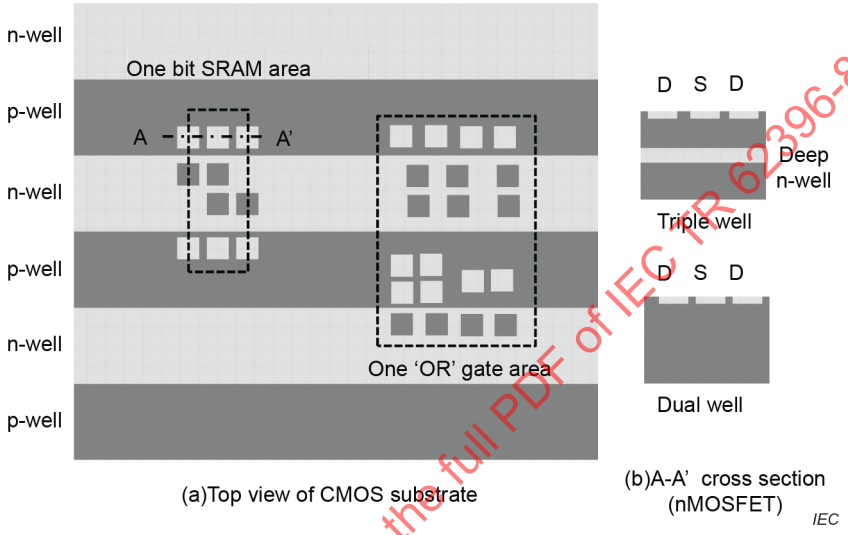

Figure A.1 – Basic substrate structure used for CMOSFET devices on the stripe structure of p- and n-wells and cross sections of triple and dual wells

Circuits are made by electrically connecting some nodes by wires above the well structure. Figure A.2 shows a typical circuit for an SRAM. Figure A.2a) illustrates a simplified expression of an SRAM, in which two inverters are connected as a ring. The circuit is stable when the data in both nodes are reversed, and thus can store data. More specifically, as shown in Figure A.2 b), two nodes Q and Q-bar store data "1" (high/V_{cc}) and "0" (low/V_{ss}), respectively. When the transfer transistors Tr_5 and Tr_6 are "ON", data on the nodes are written or read. When the state of n_1/n_2 is high, the p-MOSFET transistor Tr_4 is "Off" and the n-MOSFET Tr_3 is "On", making the state of n_3/n_4 low. This makes p-MOSFET transistor Tr_2 "ON" and the n-MOSFET Tr_1 "Off", resulting in the state of n_1-n_4 stable. Figure A.2c) shows an example of the corresponding layout of source and drain nodes n_1-n_{10}.

Logic circuits consist of a number of combinational logic gates (AND, OR, NAND, NOR), and sequential logic gates, typically FFs, as simply illustrated in Figure A.3. In synchronous logic circuits, the total operation is controlled by clock signals produced typically in PLLs. An instruction from CPUs is executed in one interval of clocks by controlling the inputs of gates between two subsequent FFs. Execution results are captured to each FF when the next clock is sent to clock the input of each FF.

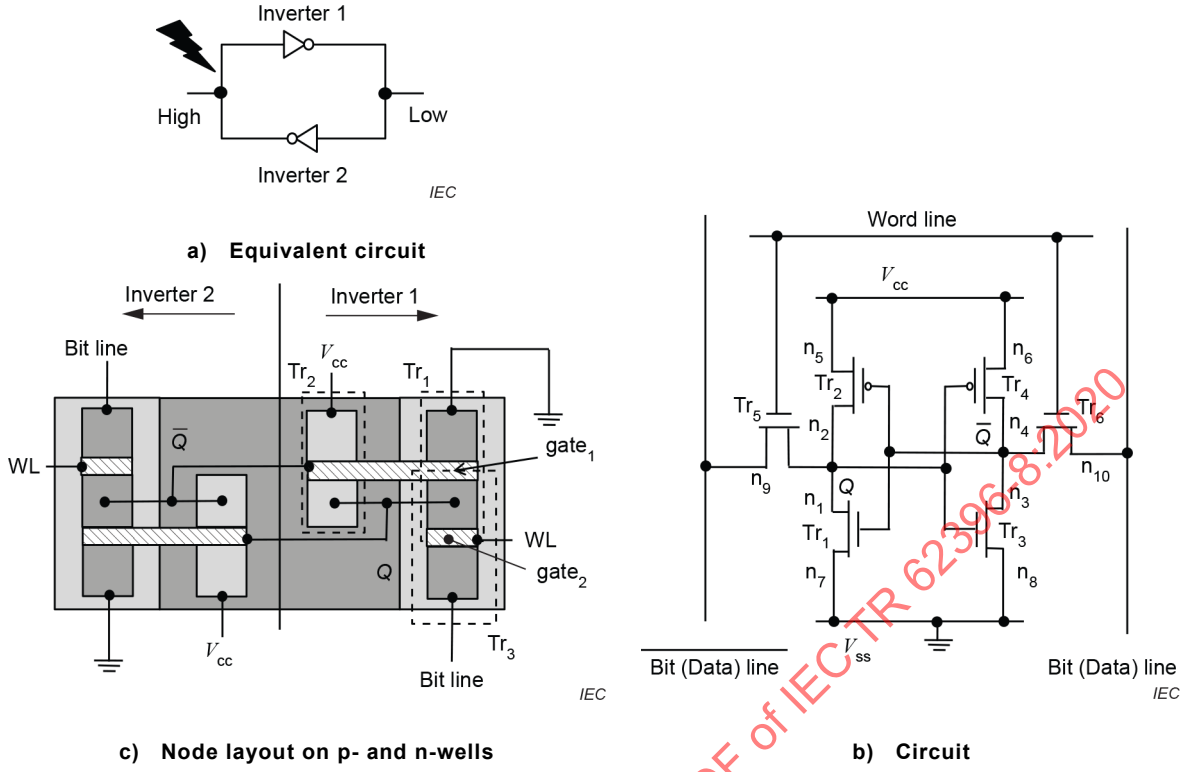

Figure A.2 – SRAM function and layout

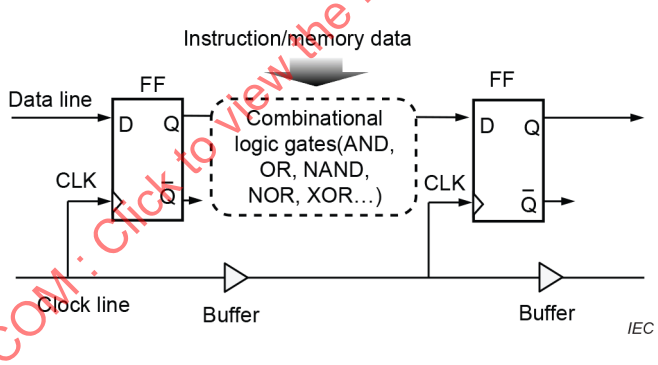

Figure A.3 – Example of logic circuit

Figure A.4 illustrates the typical architecture of an electronic system that consists of a power supply, printed circuit boards with various devices including CPU/GPU, RAM, ROM, FPGA, PLL, DSP, and IO ports, and a system like a server, router, automobile, train, aircraft and so on. Such a system can have sensors to monitor the system condition, and actuators or motors to control operation of the system. As a whole, any electronic system consists of a number of stack layers as illustrated in Figure A.5 from the lowest layer, well/substrate, to the highest layer, application or final electronic products.

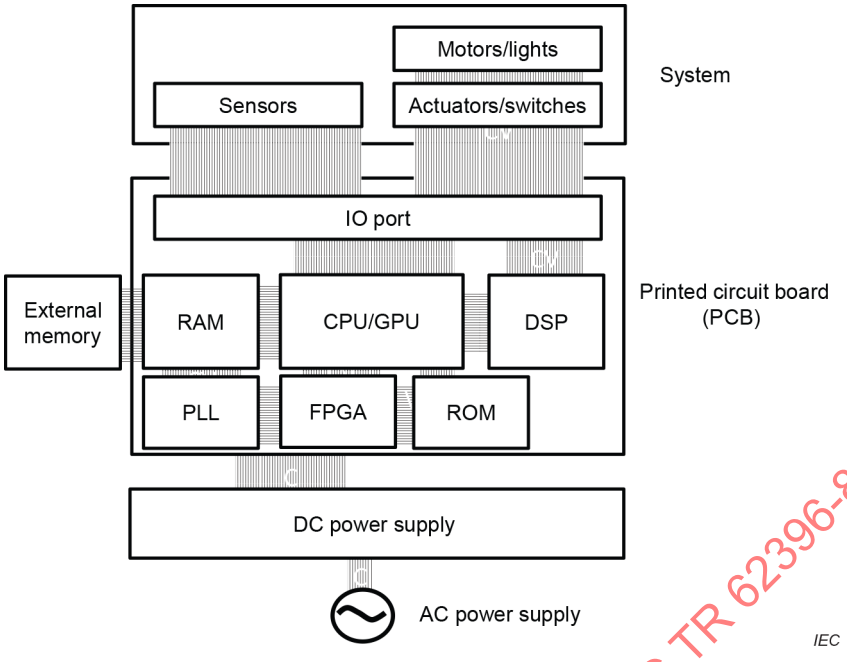

Figure A.4 – Example of electronic system implementation

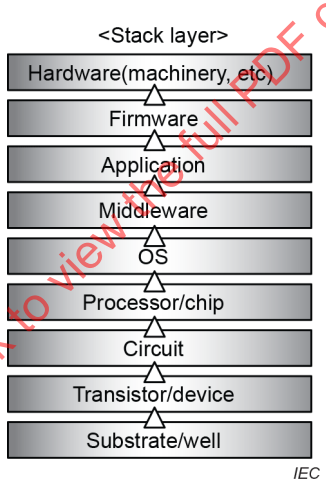

Figure A.5 – Example of stack layers in an electronic system

Annex B
(informative)

General description of radiation effects

B.1 Radiation effects in semiconductor materials by a charged particle – Charge collection and bipolar action

Figure B.1 shows a well-known representation of a charged particle interaction as it passes through an off-state n-diffusion layer, leading to the collection of a charge greater than a critical charge threshold, leading to a single-event upset.

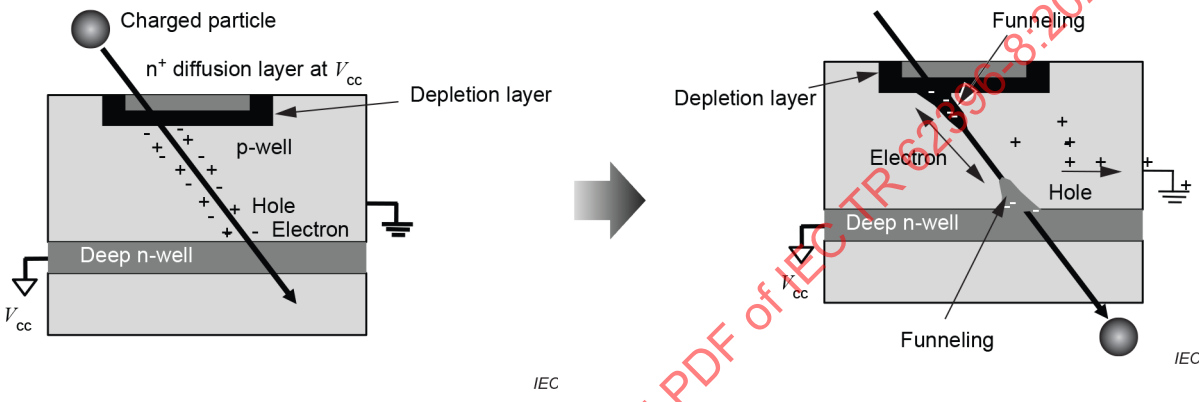

a) Ion penetration through a device

b) Charge collection at a diffusion layer and deep n-well

Figure B.1 – Charge collection in a semiconductor structure by funnelling

As the ionizing particle passes through the semiconductor device, electron-hole pairs are produced along its track. As it passes through a depletion layer, for example at the p-n junction under an off-state n-diffusion layer with potential V_{CC}, electrons generated in the depletion layer are attracted to the n-diffusion layer and holes are repulsed, flowing out throughout a ground contact. This movement of electrons and holes causes elongation of the electric field along the track such that additional electrons, produced outside the original depletion region, can be collected. This phenomenon is called funnelling [100], and is illustrated in Figure B.1b). In triple-well structures, as shown in Figure B.1b), funnelling also takes place in the p-n junction at the deep n-well, and electrons are collected on both sides.

For electronic devices with silicon feature sizes below 130 nm, Ibe *et al.* [79] have pointed out a novel soft-error mechanism, MCBI, for which passing through an off-state diffusion layer is not a necessary condition to trigger an upset as illustrated in Figure B.2. When a charged particle passes through p-n junctions in a p-well, electrons produced in the well flow out of the well and holes are left behind to make the well potential high, turning on a parasitic transistor in the well. As a substantial number of nodes are made in a single well, faults can take place in multiple nodes to cause a SET or MNT.

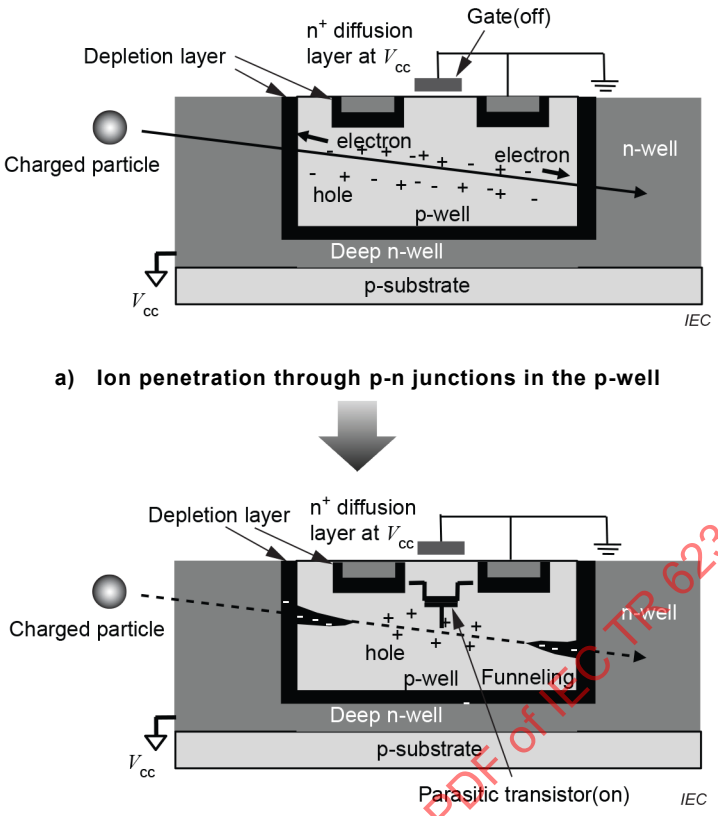

a) Ion penetration through p-n junctions in the p-well

b) Parasitic transistor is triggered by potential elevation in the p-well

Figure B.2 – Bipolar action model in a triple well n-MOSFET structure

B.2 Radiation effects by protons

As protons are charged particles, direct ionization by protons is considered [101, 45]. As protons are also nucleons, spallation nuclear reactions can also take place. Both effects can cause SEE.

For direct ionization effects, LET and range in silicon can be calculated using SRIM [102]. The results are summarized in Figure B.3 together with those for other charged particles. Since protons produced by nuclear spallation reaction with cosmic rays in the atmosphere have kinetic energies as high as a few hundred MeV, their range in silicon can be as much as a few meters.